Hue tuning curves in V4 change with visual context

Ari S. Benjamin[1], Pavan Ramkumar[2], Hugo Fernandes[2], Matthew Smith[3,4,5], Konrad P. Kording[1,2]

1. Department of Bioengineering, University of Pennsylvania, Philadelphia, PA
2. Department of Physical Medicine and Rehabilitation, Northwestern University and Shirley Ryan Ability Lab, Chicago, IL
3. Department of Biomedical Engineering, Carnegie Mellon University, Pittsburgh, PA
4. Carnegie Mellon Neuroscience Institute, Pittsburgh, PA
5. Department of Ophthalmology, University of Pittsburgh, Pittsburgh, PA

Abstract

To understand activity in the visual cortex, researchers typically investigate how parametric changes in stimuli affect neural activity. A fundamental tenet of this approach is that the response properties of neurons in one context, e.g. color stimuli, are representative of responses in other contexts, e.g. natural scenes. This assumption is not often tested. Here, for neurons in macaque area V4, we first estimated tuning curves for hue by presenting artificial stimuli of varying hue, and then tested whether these would correlate with hue tuning curves estimated from responses to natural images. We found that neurons' hue tuning on artificial stimuli was not representative of their hue tuning on natural images, even if the neurons were strongly color-responsive. One explanation of this result is that neurons in V4 respond to interactions between hue and other visual features. This finding exemplifies how tuning curves estimated by varying a small number of stimulus features can communicate a small and potentially unrepresentative slice of the neural response function.

Introduction

Neuroscience has long characterized and categorized neocortex based on the functional properties that vary across its surface. Our understanding of the visual cortex, for example, largely derives from observations that the response properties of the ventral stream ascend in complexity. V1 is discussed as responding to "edge-detecting" Gabor filters (1), V2 to variations in local curvature (2), V4 to more complex shapes (3), and IT to specific objects and faces (4), which together have inspired the theory that object recognition proceeds via hierarchical image representations (5-7).

An area's response properties are most often characterized by varying stimuli while recording activity in that area. If neural activity changes robustly along a stimulus dimension, those neurons are sometimes said to 'encode' or be 'tuned' for that feature. This approach thus relies on building a response function, or tuning curve, along one dimension of stimuli, or at most a small handful. However, natural stimuli are described by an enormously high number of dimensions. This means that there are necessarily many dimensions of stimuli that are left untested by any experiment that varies only a few dimensions of stimuli.

Leaving the response to dimensions of stimuli uncharacterized can complicate the interpretation of a tuning curve. In many studies it is hoped that tuning curves estimated from artificial stimuli will be good models of how neurons respond to stimuli in different contexts and thus represent their general functional role in visual processing. If a researcher characterizes hue tuning by presenting only colored bars, for example, they expect hue tuning to be the same for other colored shapes. For a tuning curve to be valid across multiple contexts, however, it must be the case that the dimensions of stimuli varied in an experiment do not interact with the dimensions that were not characterized, which are likely very numerous. In other words, the neural response function must be separable with respect to the varied dimension. In general, it is not clear that this is a reasonable starting assumption, and ideally it should be tested if tuning inferred from simplified stimuli is indeed informative of tuning for more complicated stimuli, like natural scenes.

In early visual areas and especially V1, there has been a large effort to characterize neurons directly from their responses to natural images (8-13). These characterizations were sometimes, but not always, consistent with those made using artificial stimuli sets. The preferred orientation of V1 neurons, for example, appears the same for both natural images and drifting gratings (11). Other aspects of the V1 response, however, are different for natural images (10), which limits how well characterizations with simple stimuli can predict the response to natural stimuli (12, 14). For higher areas like V4, however, such a comparison has not been possible. The natural scene approach popularized

in V1 requires approximating the response with a linear or second-order function of the image, but this is cannot be done accurately for V4. The nonlinearity of the V4 response is evidenced by the nonlinearity of the models that best predict V4 activity (5, 15, 16), as well as the fact that receptive fields (RFs) estimated from simple stimuli fail to predict much of the response to more complicated or natural stimuli (17-19). Without access to interpretable receptive fields estimated with natural stimuli, it has not been possible to verify that experiments with artificial stimuli sets describe how V4 responds to natural images.

Tuning curve experiments have nevertheless built a core component of our knowledge about the function and anatomy of V4. The study of its response to color has been particularly influential. V4 was first characterized as a color area (20) before later studies found selectivity for other visual features (such as orientation (21), curvature (3), shape (17, 22, 23), depth (24-26), and motion (27); reviewed in (28)). The selectivity for different visual features is spatially clustered within V4. Color-selective neurons are predominantly located in color 'globs' (29), which intersperse 'interglob' regions more selective for orientation (30). Glob cells are further arranged by their color preference (31) and generally in the same hue sequence as is found in perceptual color space (32, 33). These findings have led to a hypothesis that V4 is anatomically segregated by function. It is important to note, however, that these findings largely follow from experiments in which the stimuli were colored gratings, oriented colored bars, or other single shapes. Our knowledge of color tuning in V4, and of the functional organization of V4 more generally, is thus dependent on the experimental paradigm of varying the color of simple stimuli while observing neural activity. This leaves open the possibility that our current understanding of the functional properties of V4 are not accurate for natural stimuli.

In this work, we asked whether the hue tuning curves of color-responsive neurons in macaque V4 accurately describe their hue tuning to naturalistic stimuli. That is, we asked how well $P(Y|X, Z=z)$, which is the probability of spike counts Y given hue X and a fixed context z, stands in for $P(Y|X)$, the average hue tuning marginalized over natural images. This required developing a new method to determine how hue affects the response of a general nonlinear model of the V4 response, which in our case was based on a deep artificial network pretrained to classify images (5). We found that the tuning curves estimated from responses to stimuli of a uniform hue poorly described how hue affected responses to natural scenes. That is, $P(Y|X, Z=z) \neq P(Y|X)$. Previous conclusions about the general physiology of V4 that depended on this assumption may have to be revisited. Although hue strongly modulates the V4 response, hue tuning curves do not generalize from artificial settings to natural stimuli.

RESULTS

We recorded the spike rates of neurons in area V4 of two macaques as they viewed images on a monitor. One monkey (M1) freely viewed images as we tracked its gaze, while the gaze of the second monkey (M2) was fixed at image center during image presentation. We analyzed the responses of 90 neurons in M1 over several viewing sessions, taking care that the identity of cells on each electrode did not drift across sessions (see Methods: Session Concatenation), and in M2 recorded from 80 neurons in a single session. We then estimated tuning curves from responses to both artificial and naturalistic stimuli in order to ask if and how hue tuning generalizes.

Tuning to hue on uniform screens

We first measured hue tuning by varying the hue of a uniform flat screen (Fig. 1A). We found that many of our neurons were well-tuned to specific hues (see examples in Fig. 1B), consistent with the previous literature on hue tuning in V4 (29, 30, 32). We could consistently estimate hue tuning trials for 79/90 of neurons in M1 (Fig. 1C), but only for 17/80 neurons in M2 (Supp. Fig. 2A). A general trend across analyses was that neurons in M2 were more poorly described by hue than the neurons in M1. This difference in monkeys was possibly due to the spatial heterogeneity of color responses in V4 (29, 30).In later analyses, we compared the hue tuning of neurons only when we could reliably estimate tuning.

Next, we asked if the tuning curves of the uniform hue context could predict natural scene responses. The V4 response is complex, but if the uniform field tuning curves accurately represent the contribution of hue, and the hue response is any considerable proportion of the overall response, then they should capture at least some variance. For example, we might expect that if a neuron preferred uniform fields of orange hue (like the examples in Figure 1), then that neuron would prefer scenes containing predominantly orange hues. Instead, we found that the images that elicited the highest spike rates were often composed of consistently different hues (Fig. 1D vs. Fig. 1E). The top example in Fig. 1, for example, responded most strongly to blueish natural scenes. The bottom example represents the minority of neurons that showed a better match between uniform and natural tuning. We observed that the discrepancy between uniform hue tuning and natural scene responses was consistent across all neurons and trials (Fig 1F). Specifically, we asked how well uniform hue tuning curves could predict natural scene responses by interpreting the curves as the coefficients of a linear response to hue, and then scoring this model (see Methods). The pseudo-R^2 score of the tuning curve model

was below zero for all but one neuron (Fig. 1F and Supp. Fig. 2C), which implies that variance predicted by the uniform field tuning curves gave worse predictions than the mean firing rate on natural scenes. Knowledge of V4 responses to single hues thus does not help to predict responses on natural images.

Having observed this incongruence, we turned to considering the reason why this might occur. Hue tuning could shift between contexts, or alternatively these neurons might simply respond much more strongly to non-hue features such that the hue response is negligible. In both cases uniform hue tuning curves would explain only a small fraction of the natural scene response. To distinguish these two possibilities, we next estimated tuning to hue from the responses to natural images and compared it with uniform hue tuning.

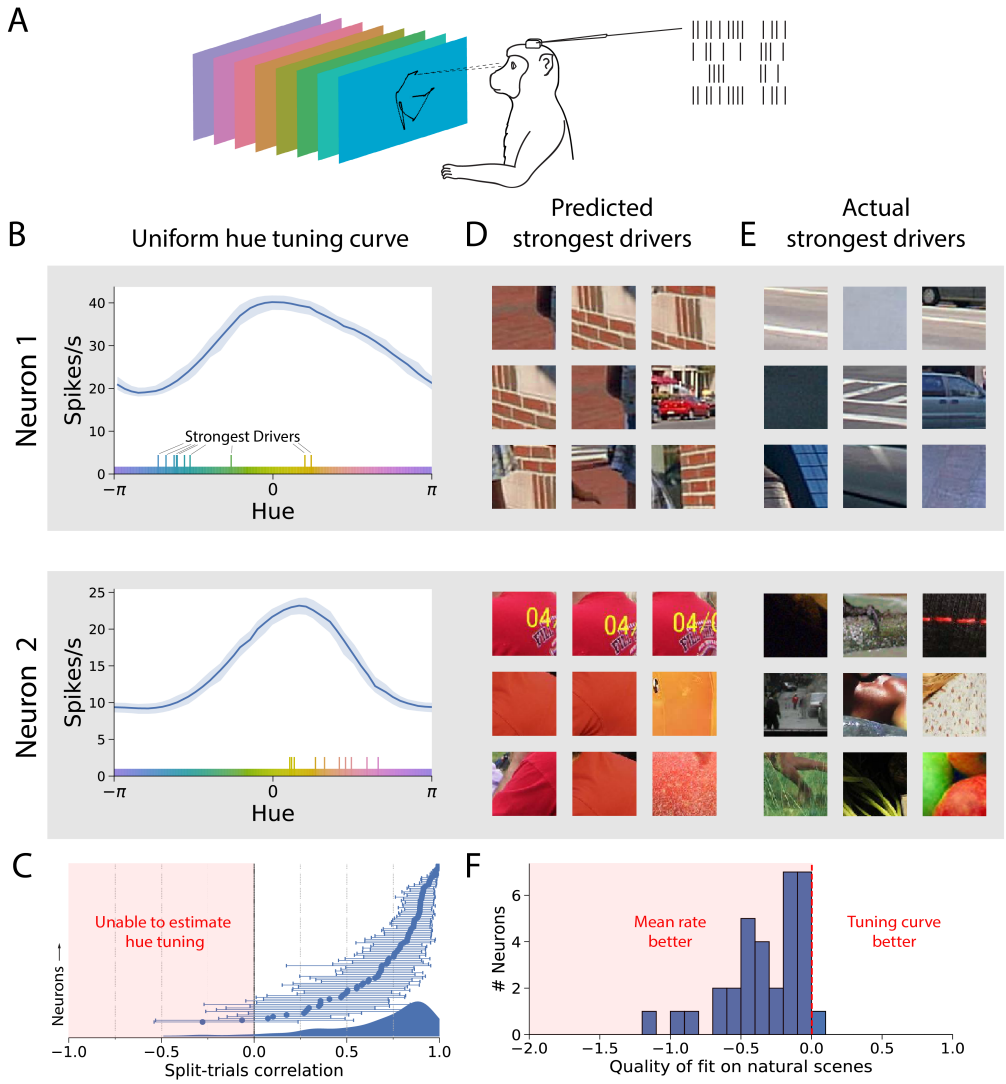

Figure 1. Tuning curves were built from responses to artificial stimuli. Data from M1; see Supp. Fig. 2 for M2. A) We recorded from neurons in area V4 as a monkey viewed fields of a uniform hue. B) The uniform hue tuning curves for two example neurons, showing strong hue modulation. C) Our ability to estimate hue tuning for each neuron was captured by the correlation of the tuning curve estimated on two non-overlapping halves of the trials. This correlation would be 1 in the no-noise or infinite-data condition. D) Using the uniform hue tuning curve as a model of V4 activity on natural scenes, we would have expected these 9 trials to elicit the strongest responses. Each image displays only the image portion within the fixation-centered receptive field. E) In reality, the highest spike rates were observed on these 9 fixations. Neuron 1's strongest drivers were dissimilar in hue from the peak of the tuning curve, while those of Neuron 2 were somewhat consistent. The mean hue of each image (weighted by saturation) is shown as a tick in panel B. F) The natural scene responses on all trials and neurons were different than would be expected from the uniform hue tuning curves. Displayed here is the histogram of the Poisson pseudo-R^2 goodness-of-fit scores of the tuning curves' predictions, which is below zero when the predictions underperform the mean firing rate.

Tuning to hue on natural scenes

In the context of natural images, one straightforward way to estimate hue tuning is to fit a (generalized) linear model to the natural scene responses using hues as covariates. In this approach, a tuning curve represents the mean change in the (log) firing rate observed with changes in each hue. This was our first and most simple method. A limitation of this model, however, is that it does not control for other visual features that drive V4 neurons, including interactions between hues. These factors will influence the hue tuning curve to the extent that hues and other features co-vary in natural scenes. To control for interaction effects, we additionally estimated tuning curves with two more complex models that each accounted for a greater number of possible drivers of V4. This progression allowed us to ensure that any discrepancy between uniform field hue tuning and natural scene hue tuning was not due to visual confounds.

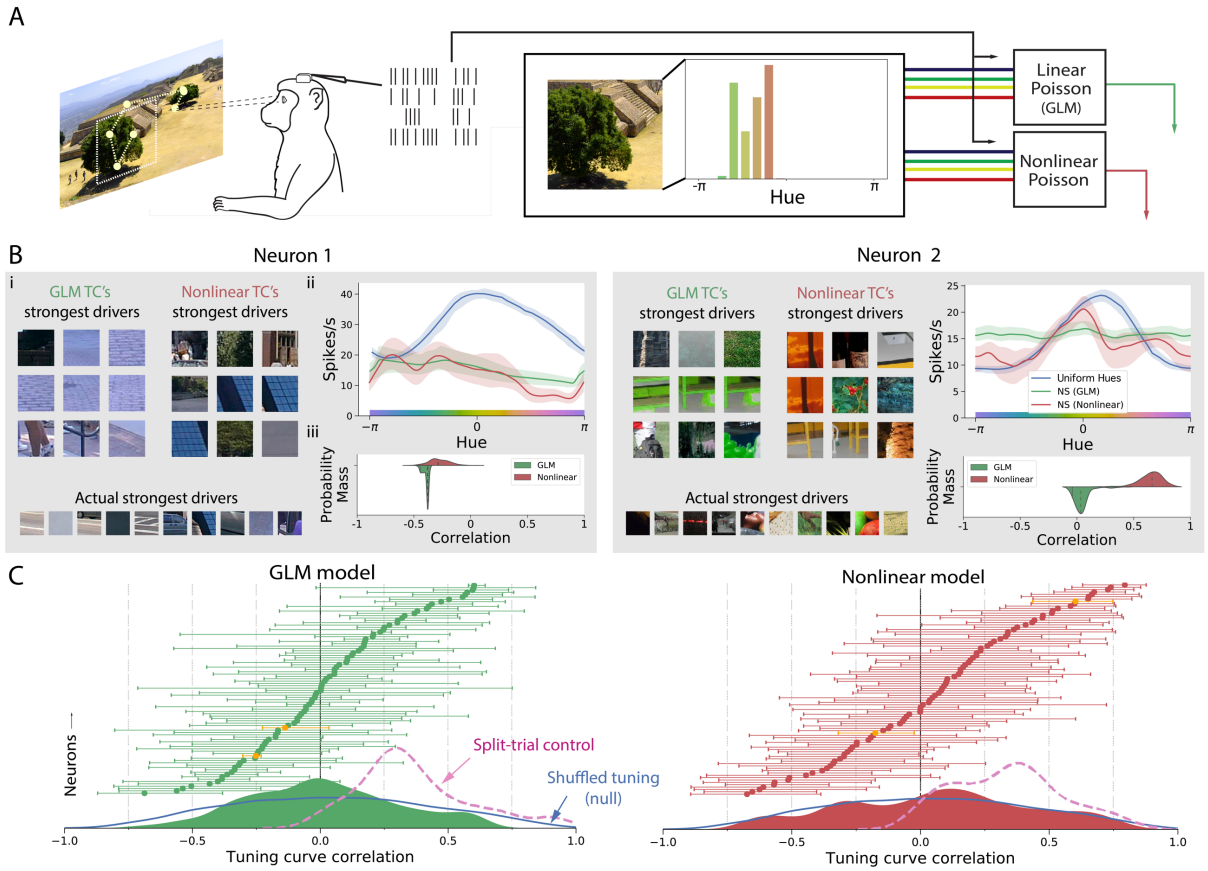

Figure 2. Tuning curves for hue were constructed from the responses to natural images. Data from M1; see Supp. Fig. 2 for M2. A) We trained two models, a generalized linear model (GLM) with Poisson output and a nonlinear machine learning model (gradient boosted trees) with Poisson output, to predict each neuron's response from the hues present in its receptive field. B) (i) The 9 trials that each model predicted to have highest firing rate looked similar to trials with the actual strongest response, unlike the uniform hue model. (ii) We built tuning curves from each model. The uncertainty of each curve is given by the 5th and 95th percentiles of hundreds of model fits to the trials resampled with replacement. (iii) This uncertainty is then propagated into the correlation between the uniform hue tuning curves and natural scene tuning curves. C) The correlations of the natural scene and the uniform hue tuning curves across all neurons show that the natural scene and uniform hue hues rarely correlate. Above: The neurons are sorted by their correlation to show a cumulative distribution. The two example neurons are highlighted in orange. The error bars on each neuron show the 5th and 95th percentiles of the distribution of correlations observed while bootstrapping over model fits. Below: The smoothed density of all neurons' natural scene/uniform hue correlations is similar to what would be expected if neurons randomly shuffled hue tuning between conditions (overlaid, blue). Also overlaid (in pink) is the control distribution, which shows how well tuning estimated from one half of the natural scene trials correlated with the tuning estimated on the other half. If hue tuning were the same across stimuli, then the distributions would look like the control distributions.

Generalized linear model of hue responses

We first modeled natural responses with a generalized linear model (GLM) upon hues (Fig. 2A). The covariates, detailed in Methods, are more specifically a histogram of the hues present in the neuron's receptive field on each fixation, with the contribution of each pixel weighted by its saturation. In monkey M2, the GLM could explain little activity (Supp. Fig. 3C), which prevented any analysis of hue tuning. (We were able to meaningfully estimate hue tuning in M2 only with our third and most complex model, below.) In monkey M1, the GLM successfully explained variance within the response to held-out natural scenes (Supp. Fig. 3B). This was a large improvement from the model estimated from responses to uniform fields. Indeed, compared to the predictions of the uniform hue tuning curves, the 9 strongest drivers of the model appeared more similar to the actual 9 strongest drivers (Fig. 2Bi). Thus, in M1, a hue model fit directly to natural scene responses provided better predictions than one fit to uniform hue responses.

The hue tuning of the GLM was measured from its responses to single hues, which is equivalent to inspecting the weights upon each hue (Fig. 2Bii, green curve). To see if hue tuning changed between natural scenes and uniform hues, we correlated the tuning curves across contexts (Fig. 2Biii). Across all neurons analyzed in M1 (Fig. 2C), the correlation between the tuning curves of the two stimuli sets varied widely and had a mean not significantly different from zero (mean of 0.01 [-0.06 0.06], 95% bootstrapped confidence interval). In fact, the spread of correlations was similar to the distribution that would arise by chance if hue tuning changed randomly between contexts (Fig. 2C inset), which we approximated by shuffling the neurons and cross-correlating their uniform field tuning curves. Thus, the tuning curves of the GLM hue model fit to natural scenes were quite dissimilar from the uniform field tuning curves.

Since the correlation across contexts would also appear to be lower due to noise or simply a bad model fit, it was important to quantify our uncertainty of the tuning estimation. We repeatedly refit the GLM on the natural scene trials resampled with replacement, and observed the distribution of coefficients. This distribution was propagated through the analysis to obtain a distribution of curve correlations (Fig. 2Biii) whose 95th percentiles form the confidence interval of the natural scene (NS) /uniform field correlation for each neuron. Since correlations of exactly 1 would be impossible in the presence of any sources of noise in curve estimation, we also visualized how high correlations would have appeared if tuning were the same in both contexts, given all sources of noise. This was estimated by comparing hue tuning on two non-overlapping halves of natural scene trials (Supp. Fig. 1A). The correlations between natural scene and uniform hue tuning were significantly lower than this control, ($p=3.2\times10^{-12}$, Wilcoxon signed-rank test; see Fig. 2C for the population distributions and Supp. Fig. 1D for the per-neuron comparison). Note that the split-trial control is a conservative lower bound of our quality of estimation, as the model was fit on only half the number of trials. Thus, uncertainty in our curve estimation cannot explain away our observation of a difference in the hue tuning of the GLM fit to natural scenes and uniform hue tuning.

Nonlinear model of hue responses

A shortcoming of the GLM is that it does not model interactions between hues. Nonlinear hue interactions have been previously observed in V4 (34). This would lead to a bias in the GLM's hue tuning because hues are correlated in natural scenes (Supp. Fig. 3A). To test if this bias could explain the observed difference in hue tuning, we fit a second model that included nonlinear interactions between hues. We fit a machine learning model (gradient boosted decision trees, via XGBoost) to predict the neural response from the histogram of hues present in each natural image fixation. This model, which we refer to as the 'nonlinear hue model', predicted neural activity more accurately than the generalized linear hue model for all neurons in both M1 and M2 (Supp. Fig. 3B,C). This confirmed that these neurons responded nonlinearly to hue. It is important to note that because of this nonlinearity, no one-dimensional tuning curve could represent the full hue response. It would be necessary to estimate multi-dimensional hue tuning curves to display interactions between hue bins. Our focus here is instead on the average response to individual hues on natural scenes, and whether this average hue response was similar to hue tuning on uniform hues.

We estimated hue tuning curves for the nonlinear hue model fit on natural scene responses by measuring its responses to single hues, in essence reproducing the uniform hue experiment but on the natural scene model. If hue tuning were the same between contexts, then the tuning curves of this model would be the same as the tuning curves of the neurons estimated on uniform hues. In neurons for which we could consistently estimate hue tuning, we found that these tuning curves correlated poorly with the uniform field tuning curves (Fig. 2B,C). However, they correlated strongly with those estimated from the GLM (Supp. Fig. 4A), indicating the bias due to nonlinearity and hue correlations was small. As we did for the GLM, we estimated our ability to estimate tuning by correlating tuning curves estimated on non-overlapping halves of data. The nonlinear hue model was able to consistently estimate hue tuning for many neurons in M1 (Fig. 2C overlay) but for just two neurons in M2 (Supp. Fig. 2 D-F), which prevented a statistical analysis in M2. In M1, the natural scene/uniform field tuning curve correlations were significantly lower than these split-trial

correlations ($p=1.0x10^{-14}$, Wilcoxon signed-rank test; Supp. Fig. 1D), indicating that the observed change in hue tuning across contexts was not a consequence of noise in the estimation of tuning. Thus, even after accounting for interaction effects between hues, our key finding – that uniform field tuning does not generalize to natural scenes – is consistent across models.

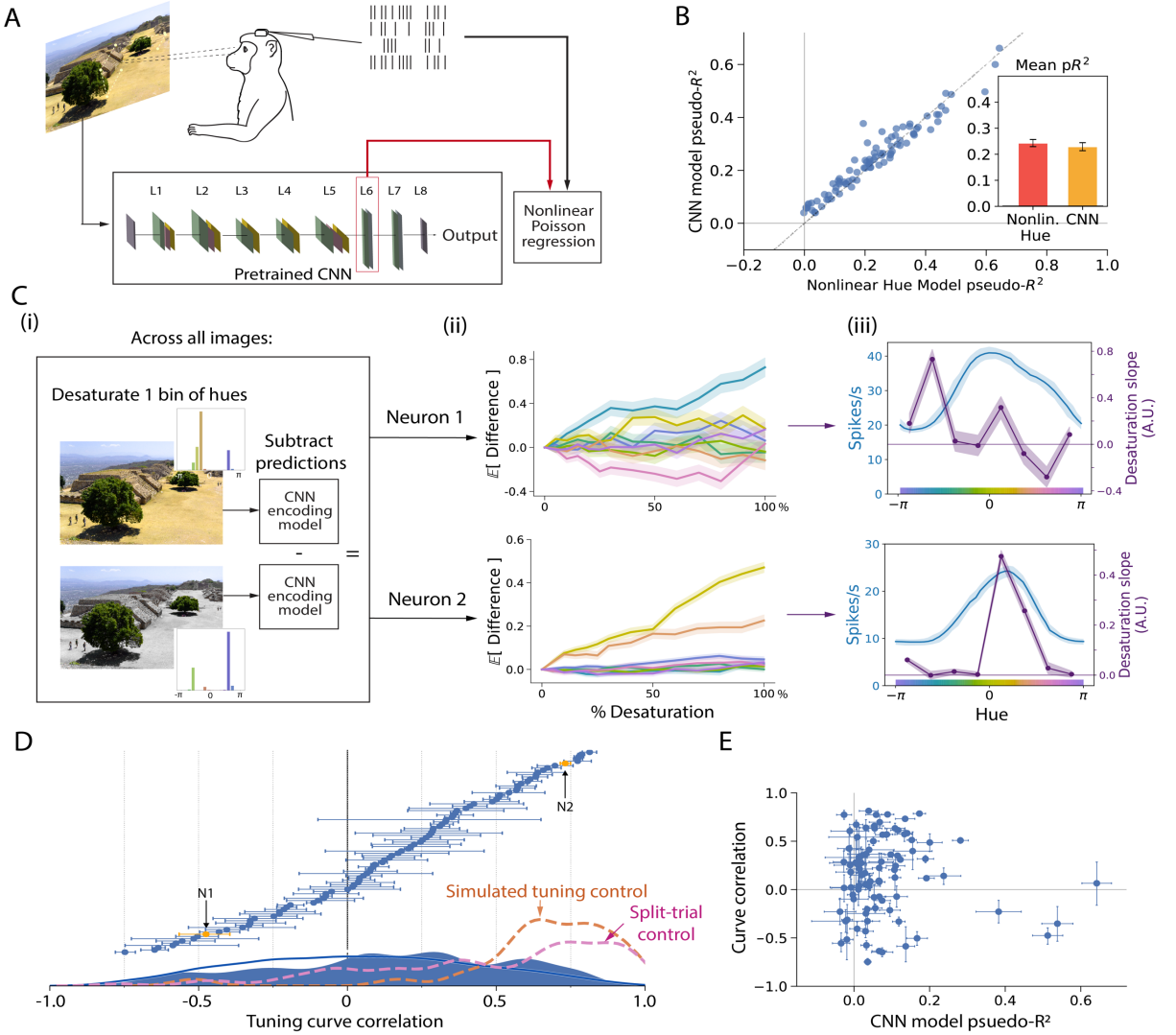

Figure 3. A model of V4 responses was built from a pretrained convolutional neural network (CNN), which we then used to build tuning curves for hue. Data from M1; see Supp. Fig. 2 for M2. A) We trained a nonlinear Poisson regression model (gradient boosted trees) to predict the V4 response from the activations of an intermediate layer in the VGG16 network given the visual stimulus. B) The quality of the neural predictions on each neuron, measured by the cross-validated pseudo-R^2 score, were similar between the CNN model and the nonlinear hue model. C) We built hue tuning curves in the following manner: (i) For each image in a test set, we slightly desaturated all pixels in a bin of hues, and subtracted the CNN model's predictions on the perturbed image from those on the original image. (ii) For each neuron, the average change in the predicted response across all test images was plotted against the percentage by which hues were desaturated. The slope of each line is, to first order, the average effect of that hue on the model response in the test set. The top and bottom plots show the same example neurons as in earlier plots. (iii) The resulting tuning curve (purple) summarizes the average effect of each of the 8 bins of hues – i.e. the slopes of the 8 desaturation curves. It can be seen that the tuning of neuron 1 was poorly correlated with the uniform hue tuning (blue), while that of neuron 2 was well-correlated, in agreement with the hues of the strongest-driving stimuli shown in Fig. 1B. D) We calculated the correlation between the two tuning curves for all neurons. The distribution of correlations was lower than for the reconstructed hue tuning of simulated neurons ("simulated tuning control"; see also Supp. Fig. 5) as well as the distribution of correlations between tuning curves estimated from two non-overlapping halves of the natural scene trials ("split-trial control"; see also Supp. Fig. 1). E) The quality of the CNN model fit for each neuron did not predict the correlation of the tuning curves.

Neural network model of V4 responses

We next repeated the estimation of hue tuning on natural scenes with a more general model of V4 neurons that does not rely on hand-specified summaries of the features present in a receptive field. This was important to ensure that our results were not sensitive to design decisions in processing the images, as well as to account for the confounds of other, non-hue features contained in the image. The model we selected was based on a recent encoding model of V4 that relates neural responses to the activations to the upper layers of a convolutional neural network (CNN) pretrained to classify images (5). Such "transfer learning" models have also recently been used to infer optimal stimuli for neurons in V4 (15, 16). Our model took an entire fixation-centered image as input, ran it through the network, and then the network activations were used to predict each neuron's response with a classifier trained for each neuron (Fig. 3A). The predictions of neural activity given by this model were comparable in accuracy to those of the nonlinear hue model, indicating that the neurons predominantly responded to hue and that the nonlinear hue model was a good simplified description (Fig. 3B). The CNN model of V4 comparably predicted the activity of neurons despite making many fewer assumptions about how raw pixels related to responses.

This learned V4 model has several advantages over the linear and nonlinear models predicting activity from hue statistics in the estimated receptive field. First, instead of having to pre-specify a receptive field or estimate one with sparse noise, we allowed the CNN model to learn any location sensitivity itself and thus fed the entire fixation-centered image as input. The CNN model could also model the interactions of hue with spatial features. This allowed us to control for non-hue confounds. The linear and nonlinear hue models would provide biased estimates of tuning if neurons also responded to other visual features, and if these features co-varied in the image dataset with hue. If most green objects are plants, for example, the observed dependence on green hues may be partially attributable to a response to the high spatial frequency of greenery. Theoretically, one could include these features as additional covariates, but the list of features that drive the V4 response in a simple manner (e.g. linearly) is not comprehensively known. Good progress has been made with shape and texture (3, 35, 36), but arguably not enough to thoroughly control for all non-hue features in a simple model. The CNN model circumvented this problem by learning the relevant visual features rather than requiring that they be chosen by a researcher, parameterized by hand, or written out.

We developed a novel method to estimate hue tuning from a general encoding model like the CNN model. We found we could not simply observe the model's response to images of a uniform hue, as before, because this approach failed to reconstruct tuning on simulated data. This interesting parallel to our main finding is likely due to feature interactions in the model and the fact that uniform field test images are far outside the domain of natural scenes on which the CNN was pretrained. Instead, we estimated the effect of hue by slightly perturbing the hue of input images and observing the change in the learned model's response (Fig. 3C). First, for a test set of images not used for training, we desaturated all pixels within a bin of hues by a set percentage (Fig. 3Ci). The percentage of desaturation varied from 0% (i.e. no change) to 100% (in which all pixels of one hue are taken to isoluminant grey). We took the difference between the model's predictions on the original and perturbed images and examined how severely this difference depended on the level of desaturation (Fig. 3Cii). For each neuron, we averaged over the entire image dataset to yield the average hue tuning on natural images. Finally, to build the tuning curves, we calculated the slope of the desaturation curve for each hue (Fig 3Ciii). This method established the effect of hue only in the tight neighborhood of each image, and is set up to estimate the average local effect of hue on the natural image response.

To ensure that this process could in principle reconstruct correct tuning curves, we built simulated responses (Supp. Fig. 5). We generated random cosine tuning curves, then simulated a hue response by applying these as linear filters upon the histograms of the hues present in each image. We then attempted to predict these simulated responses from the activations of the pretrained CNN given the raw images. Using the method of progressively desaturating test images, we found we could reconstruct the original cosine tuning curves with high accuracy (Fig. 3D overlay and Supp. Fig. 5), even though the pretrained CNN model was trained to classify images and not to extract hues. As a second, more conservative test, we also performed the split-trial control for the actual V4 neurons, which involved repeating the entire analysis separately on two non-overlapping halves of natural scene trials and then correlating the two resulting tuning curves. The split-trial tuning curves showed significantly positive correlations for most neurons in M1 (Fig. 3D overlay) as well as for neurons in M2 (Supp. Fig. 1). This method of querying the effect of hue could thus accurately estimate hue tuning curves from natural scene responses in both monkeys.

We next asked if these tuning curves would be different than tuning curves to uniform hues. We found that the tuning curves of one context were different from tuning in the other (Fig. 3D for M1 and Supp. Fig. 2I for M2), as for the previous models. If hue affected V4 responses in the same way in both contexts, we would have observed the correlations to be at least as positive as the split-trial control. This was not the case. Among those neurons for which

we could consistently estimate hue tuning, the natural scene/ uniform hue tuning curve correlations were significantly closer to 0 (Supp. Fig. 1D for M1; Supp. Fig. 2I for M2). This difference in tuning curves was not an artifact of our model fit or estimation method, as this would be measured in the split-trial control, and additionally we observed no correlation between the model's accuracy on unseen natural images and the natural scene/uniform field correlation (Fig. 3E and Supp. Fig. 2K). In addition to changes in tuning curve shape as captured by correlation, we also examined if the natural scene tuning curves showed changes in the overall degree of hue modulation. We found that hue modulation – the maximum of a tuning curve minus the minimum, normalized by the mean – was related across contexts, but weakly (Supp. Fig. 6). Many neurons strongly modulated by hue on uniform fields had weak responses to hue on natural scenes, and vice versa. Overall, the tuning curves estimated with this more advanced method support our previous conclusion that hue tuning on uniform fields does not agree with the effect of hue in natural scenes.

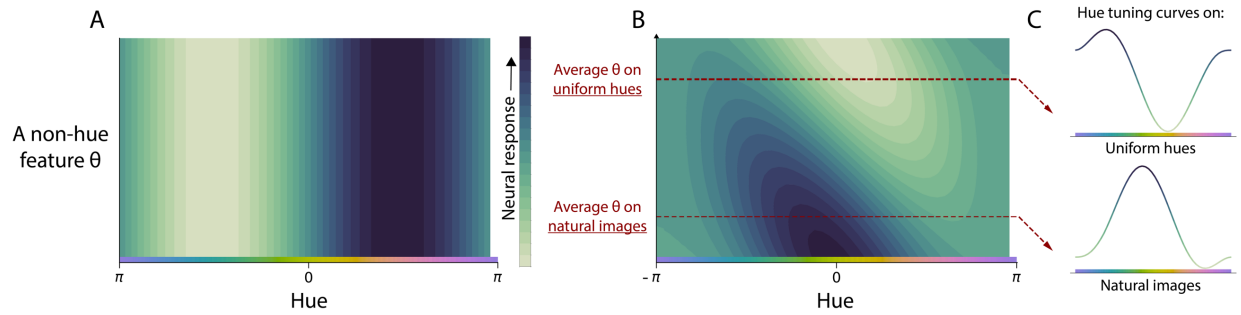

Figure 4: Interactions between features allow neurons to carry more information in their activity, at more times. A) In this two-dimensional tuning curve, a hypothetical neuron responds to only hue and carries no information about other variables. B) A hypothetical neuron that responds as well to another non-hue feature is informative about multiple dimensions of stimuli (due to its nonzero derivative). C) We can build a hue tuning curve for this neuron by varying hue with the other feature held fixed. If the average non-hue feature is different between natural images and uniform hues, the tuning curves to hue will differ between contexts.

Why interactions between features?

A straightforward explanation of why hue tuning differs across visual contexts is that these neurons respond to nonlinear combinations between hue and non-hue features, as shown schematically in Figure 4. There must be a computational advantage that explains this coding scheme for visual perception. It is clear that if the role of these neurons were to encode hue alone, then any nonlinear interactions would be detrimental. This is because hue can no longer be unambiguously read out without additional contextual information. Therefore these V4 neurons likely assist in a more general task, like object recognition or segmentation. Other studies have also noted that color vision may be best thought of in terms of task performance; the absorbance spectra of the L and M photoreceptors in primates, for example, are not maximally separated as in birds but rather overlap significantly, likely because this helps to discriminate and classify fruit and leaves (37). The question then arises: why would neurons being responsive to multiple features help visual processing?

A simple strategy that predicts nonlinear interactions is to minimize the error of any read-out of encoded information from V4 to other brain areas. We can make this idea precise by referring to the notion of Fisher information, which bounds the mean squared error of any optimal readout from population activity (see Supplementary Information for additional details). This framework pulls from a large literature relating to optimal coding strategies (38-40). The Fisher information is higher – and the potential decoding error is lower – when the neural population activity is highly sensitive to changes in the task-relevant features. One way to increase the population sensitivity to the task (i.e. the Fisher information) is to have each neuron be sensitive to multiple features. This will increase the total number of neurons in the population that are sensitive to each feature; when each neuron responds to k features instead of just one, k times more neurons respond to each feature on average. By increasing this number, the Fisher information also increases (though see below), and the minimum achievable error on the task decreases.

Eventually, however, further increasing the k number of features to which a neuron responds will deteriorate how precisely it can respond to other features, decreasing the Fisher information. Depending on neural physiology (for example, the maximum firing rate, synaptic noise levels, and correlated variability), this tradeoff determines the optimal number of features that a neuron should respond to. It is an extreme and unlikely case when the optimal number is one. Indeed, several publications have found that in common scenarios, like linear-nonlinear responses (39)

and von Mises tuning curves (41), feature interactions are usually optimal. In particular, some degree of interaction is always optimal when the features co-vary in the natural world. This is the case with hue and most visual descriptors, and so it could be expected that V4 neurons would show interactions between hue and other visual features.

DISCUSSION

For populations of V4 neurons in two macaques, we tested if tuning curves measured from simple stimuli of uniform hues would accurately describe hue tuning measured from natural scenes. We found that hue tuning for uniform hues was not informative of hue tuning estimated directly from natural scene responses. This finding was robust across multiple methods of estimating tuning, which together accounted for the confounds of both hue-hue interactions as well as of non-hue drivers of V4 activity. This was accomplished by measuring the hue tuning of a general, neural network-based encoding model by slightly perturbing the hue of test images. A hue tuning curve for V4 estimated from any one set of stimuli thus does not universally describe the average response to hue on other stimuli. This implies that V4 neurons, including those with strong hue modulation, respond to nonlinear combinations of hue and non-hue information.

This finding is in line with data from a recent study in V4, which searched for an interaction between shape and color in the responses to a range of simple shapes (42). The authors observed that, in a linear model, there was a significant interaction between shape and color in the majority of cells (51/60), and that when modeling this interaction as a color-dependent gain on shape tuning, most cells (44/60) showed nontrivial gain. In those cells, as well as ours, the stimulus/response function of V4 neurons could not be separated simply (e.g. multiplicatively) into a function of hue and a function of other stimulus variables. Accurately characterizing tuning curves that are applicable to natural images thus requires considering nonlinear interactions between features.

Known sources of modulation in visual responses

The V4 response is modulated by a number of factors that change with visual context. These factors are divided in the manner of their relevance to our findings. First are those factors that could act as confounds upon the estimation of hue tuning on natural scenes but were not fully controlled for. These are possible reasons why we might have observed low tuning curve correlations even if, in fact, tuning did not change between contexts. The second category of factors are known interactions between hue and other features in the V4 response. These are possible explanations of why hue tuning in V4 changes with visual context. We will review both in turn.

Of first concern as a potential confound upon hue tuning estimation is visual attention (43). A particularly relevant form of attention is feature-based attention, in which neurons tuned for a feature (say, red) increase their firing rate if that feature is attended to (as in the task, “find the red object”) (44, 45). While our task was free viewing and involved no instructions, it is likely that the monkey’s attention shifted during the task and that it was influenced by object salience. This effect may bias our results if object salience were correlated with hue. It is plausible, for example, that figures were more salient than ground (e.g. see (46)) and that certain hues were more common in the background than others. We have not directly controlled for attention, apart from trends in salience that might have been learned by the CNN model, but we believe that the size of the apparent change in hue tuning cannot be attributable to salience-hue correlations.

Neurons in V4 are have been shown to preferentially respond to objects near the center of attention, even when attention falls away from fixation (47-49). This phenomenon of receptive-field remapping is most problematic for our GLM and nonlinear hue models, which required that we extract the hues lying within the receptive field. If the monkeys’ attention frequently strayed away from fixation, we would have extracted hues from an irrelevant image portion. This would introduce some noise in the hue covariates, and therefore some smoothing of hue tuning curves. The CNN model learned any spatial sensitivity directly from the natural scene responses instead of from previous characterizations with sparse noise stimuli. However, the effect of attention upon receptive fields could not be modeled and it is likely that some smoothing of the hue tuning curve occurred for this technique as well. Smoothing would obscure fine-scale structure in the tuning curves. As the curves were already smooth, however, the natural scene/uniform field correlations should not be much diminished. The smoothing effect is furthermore not consistent with our finding that many neurons have natural scene hue tuning with zero, or even negative correlation with their uniform field tuning while still showing strong hue-dependent modulation. The dependence of receptive fields upon attention may explain some decrease in correlation, but cannot explain the entire difference in the estimated effect of hue across contexts.

We now turn to potential descriptions of the interactions that might have led to a shift in hue tuning across contexts. One possibility is color constancy, in which neurons respond to the inferred surface color of objects rather than their

apparent color (which reflects the color of ambient light) (34). This is a clear example of the nonseparability of the V4 response to hue, and a reason hue tuning might change between any two, single stimuli. It is less obvious, however, that color constancy would cause the average effect of hue over all natural images to be different than on uniform hues. It would be expected that over tens of thousands of images with broad range of lighting conditions, color constancy would result in some smoothing of the estimated tuning curve due to the difference between the pixels' hue and the inferred hue, and of the same characteristic scale as the typical difference. More concerning is the bias that would result from the discrepancy between pure white and the average lighting condition. We expect this discrepancy to be small, and therefore natural scene tuning curves would still be strongly (though not perfectly) correlated with the uniform field tuning curves. Though color constancy would affect hue tuning on natural scenes, it cannot account for the entire difference we observed, and it is likely that there exists other undocumented sources of nonseparability.

A subpopulation of neurons in V4, so-called equiluminance cells, respond to object boundaries defined solely by chromatic boundaries (50). Such shapes are defined by changes in hue or saturation, and so it is worth asking whether the response function of equiluminance cells includes interactions between hue/saturation and spatial arrangement. However, it was not originally determined if the responses were actually separable in this way, as neurons' hue tuning curves were characterized with a fixed shape. It is possible that equiluminant cells had fixed hue tuning that was then modulated by shape. Thus, it is plausible but undetermined that equiluminance cells would show different hue tuning across shape and explain our results.

Implications for V4 and for the tuning curve approach

Color responsivity has long been a defining feature of V4 (20, 51). Recent studies have shown that localized areas in V4 are strongly responsive to color (29), and furthermore that the anatomical organization of color preference on the neocortex is similar to perceptual color spaces (31-33). These findings have been taken as evidence that areas within V4 are specialized for the perception of color. However, each of these studies characterized hue tuning by changing the color of simple shapes. Since the color tuning of V4 neurons changes with visual context, as we show here, it is possible that previous conclusions about the functional organization of V4 do not accurately describe how V4 processes more naturalistic stimuli. Studies of the spatial organization of hue tuning should be re-evaluated using multiple classes of stimuli.

Some previous studies, based on the discovery of robust tuning for the color of simple visual stimuli, have concluded that the role of color-responsive areas in V4 is to represent color. Our results do not rule this out; for example these areas might represent color but be modulated by what colors are likely given the surroundings. This would complicate a read-out of color from V4, but may have other advantages like efficiency. However, it could also be that the color-sensitive areas of V4 are not specialized to represent color, *per se*, but rather serve a more complex role within recognition and perception. This is analogous to how V2 appears tuned to orientation, but can perhaps be better described as processing naturalistic texture (52). Furthermore, this role aligns with the suggestion that the ventral temporal cortex at large decomposes scenes into neural activity such that object categories are linearly separable (53). Thus, the color-responsive areas of V4 may represent how color informs an inference of object identity. Whether the color responses of V4 are an end to themselves (i.e. representing color) or intermediate computations in a larger assessment of object identity, or both, cannot be decided from this study; both are consistent with the data.

Our study joins a longer history of literature observing that, across many brain areas, tuning curves previously characterized with simple stimuli in fact change with context. In V1, for example, researchers found that receptive fields change with certain visual aspects that were not varied within previous stimuli sets, such as the presence of competing orientations in the classical receptive field (54) or outside of the classical receptive field (55-57). Even sound has been shown to modulate V1 receptive fields, at least in mice (58). More recently, it was observed that receptive fields are different in the contexts of dense versus sparse noise for neurons in layer 2/3 of V1, though are similar in layer 4 (59). Spatio-temporal receptive fields of V1 neurons also appear different when estimated on natural movies versus drifting gratings (10, 12) (though note that orientation tuning is similar for static natural scenes versus gratings (11)). In other areas, such as for retinal ganglion cells (60, 61) and in macaque M1, S1, and rat hippocampus (62), contextual modulation in the form of nonlinear feature interactions have been identified by comparing the performance of a model that assumes separability (such as a GLM) with a nonlinear model that does not. Thus, while tuning curves generalize in some situations (e.g. (11)), it is common that they do not, and any assumption of separability of the neural response should be verified. Furthermore, as discussed in Results and the Supplementary Information, feature interactions are likely optimal for visual processing when the full visual scene is represented in neural activity and should be expected. Unless specifically investigated, it might not be correct to assume that a tuning curve accurately describes the neural response on different stimuli than used to create it.

This conclusion has a concerning consequence for visual neurophysiology. If it cannot be assumed that neural tuning is separable, it becomes necessary to test prohibitively many stimuli or else make an alternative simplifying assumption. This is because the stimuli must scatter the entire space of relevant features, rather than be systematically varied along just one feature at a time. Since the number of tested stimuli must follow the number of potential feature combinations, the overall number of stimuli will grow exponentially with the number of features. When there are very many features, even very large recording datasets by today's standards may be insufficient.

One possible way forward is to make simplifying assumptions, i.e. to set strong priors of the kinds of tuning curves that could be expected. This is the approach taken, for example, when modeling neurons using the activations of deep neural networks pre-trained on image classification tasks (5, 63) or considering neural responses as implementing a sparse code (9, 64). To compare with the previous literature, single dimension experiments can then be performed on these complex encoding models, as we demonstrate here, or alternatively performed directly on artificial neural networks to gain intuition about what tuning curves say about information processing (65, 66). In general, finding suitable priors will require the use of strong theoretical ideas and mechanistic hypotheses. To estimate tuning without assuming separability, then, neurophysiology must embrace and develop theories of neural processing.

METHODS

Experimental setup: recordings

In each of two monkeys, we recorded from 96-electrode Utah arrays (1.0 mm electrode length) implanted in visual area V4. Surgical details describing the implantation method can be found in previous publications (67, 68). The array was located in the left hemisphere for monkey M1 and in the right hemisphere for M2. Spikes were sorted off-line first with an automated clustering procedure (69) and then refined by hand using custom MATLAB software (https://github.com/smithlabvision/spikesort) taking into account waveform shape and interspike interval distributions (70).

All experimental procedures were approved by the Institutional Animal Care and Use Committee of the University of Pittsburgh.

Gaze tracking and fixation segmentation

We employed a free-viewing paradigm for one monkey (M1) and a fixed-gaze paradigm for the other (M2). The location of each monkey's gaze on the screen was tracked with an Eyelink 1000 infrared tracker (SR Research, Ottawa, Ontario, Canada). Visual stimuli were presented and the experimental trials were controlled by custom Matlab software in conjunction with the Psychophysics Toolbox (71). For monkey M1, we segmented each fixation as a separate event based on thresholding the position and velocity of the gaze coordinates. We did not analyze activity occurring during eye movements. Once each fixation was separated, the average location of the fixation was recorded and matched to image coordinates. Monkey M2 was trained to fixate on a dot positioned at the center of each image. The gaze was tracked as for M1, but this time only to enforce fixation and terminate the trial if the gaze shifted away from center.

Artificial stimuli

Both monkeys viewed uniform images of a single hue on a computer screen at 36 cm distance, with a resolution of 1024x768 pixels and a refresh rate of 100 Hz on a 21" cathode ray tube display. The full monitor subtended 55.5 degrees of visual angle horizontally and 43.1 degrees vertically. The monitor was calibrated to linearize the relationship between input luminance and output voltage using a lookup table. This calibration was performed for grayscale images, and the color profile of the monitor was not separately calibrated. The hues were sampled from the hue wheel in CIELUV color space at increments of 1 degree, and were presented in random sequence. Monkey M1 freely viewed the stimuli, and was rewarded periodically for maintaining eye position on the screen for 4 seconds, after which time the static image was refreshed. The trial was ended if the monkey looked beyond the screen during this duration. Monkey M2 was trained to fixate a small dot at the center of the screen for 0.3 seconds, during which three images were flashed for 100ms each. A 0.5 second blank period interspersed each fixation. Monkey 1 viewed 7,173 samples of the uniform hue stimuli over 10 sessions, while Monkey 2 viewed 1,119 samples during a single session.

Natural images

Both monkeys viewed samples from a dataset of 551 natural images, obtained from a custom-made Google Images web crawler that searched and downloaded images based on keywords such as cities, animals, birds, buildings, sports, etc. Monkey M1 viewed images over 15 separate sessions, for a total of 77961 fixations. Monkey M2 viewed images over two sessions on a single day, for a total of 6713 fixations. We then extracted the features from the image patch centered around each fixation that would serve as model inputs. The image patch around fixation corresponded to the 200 x 200 pixel block surrounding the center of gaze. This corresponds to a region subtending the central 11.7 square degrees of visual angle.

For the nonlinear methods we included a small number of features unrelated to the images as additional controls. To account for possible stimulus adaption, we included the trial number in the session and also the number of times the monkey previously fixated on that image. While all models predict the spike rate, which is already normalized by the fixation duration, we included the fixation duration as an input to control for possible nonlinearities of rate with fixation duration. We also included the duration of the saccade previous to the current fixation, the duration of the saccade after fixation, the maximum displacement of the gaze position during the entire duration of the fixation, and whether the pupil tracking was lost (often due to a blink) in the saccade before or after fixation. Including these inputs allowed the nonlinear methods to control for factors which also may affect spike rate.

Receptive field estimation

To estimate hue tuning on natural scenes with the hue models, we needed to know which hues were present within the RF on each fixation. We mapped the RFs by presenting sinusoidal gratings at four orientations, which were flashed sequentially at the vertices of a lattice covering a portion of the visual field suggested by anatomical location of the implant. We then extracted the hues present in the 50x50 pixel block surrounding the centroid of the RFs of each monkey. The location of the RF was confirmed in the natural scene presentations as the pixel block that allowed the best predictions on held-out trials.

We did not use this RF information in the CNN model, which took as input the entire image region around the fixation. Since information about spatial location preserved in the lower and intermediate layers of the CNN, the RF for any neuron can be learned. This addressed any worry that the RF specification might systematically change for natural images.

Session concatenation

Although all recordings in M1 were performed with the same implanted Utah array, they were recorded over several sessions. The recordings for M2 were made in a single session. In M1, this introduced the possibility that the array might have drifted, and that a single channel might have recorded separate neurons in different sessions. To address this possibility, we noted that spikes identified in a channel in one session will be less predictive of another session's activity if the neurons are not the same, as we expect tuning to be relatively static across days (72, 73). We thus filtered out neurons whose uniform hue tuning changed across sessions. We trained a gradient boosting regression model with Poisson targets to predict spike counts in response to the hue of the stimuli. Nuisance parameters, such as duration of stimulus, gaze position, inter-trial interval, etc., were also included as model covariates to increase the predictive power even for neurons that were not hue-tuned. We then labeled a neuron as having static tuning as follows. First, we trained the model on each single session in a 10-fold cross-validation procedure and recorded the mean pseudo-R^2 score. This score reflected how well the model could predict held-out trials on the same session. Then, we re-trained the model on each session and predicted on a different session, for all pairs of sessions. This resulted in a cross-prediction matrix with diagonal terms representing same session predictability (the 10-fold CV score), and off-diagonal terms representing generalization between sessions. We did not concatenate sessions if there was not significant generalization between them.

The natural image sessions were interspersed with the artificial sessions. If a natural image session occurred between two artificial sessions, and a neuron showed static tuning both artificial sessions as identified in the above manner, then that natural image session was included for the hue tuning comparison and model fitting. The recordings of units from other natural image sessions were not used. This procedure improved our confidence that the neurons recorded in different sessions were the same.

Uniform hue tuning curve estimation

Hue tuning curves were built for each neuron by plotting its spike rate on each fixation against the observed hue. For the visualizations in the figures, we performed LOWESS smoothing, in which each point of the curve is given by a locally-weighted linear regression model of a fraction of the data. The error envelope of the curve represents the 95% confidence interval given by bootstrapping over individual fixations. To calculate the correlation between tuning

curves, we did not correlate the LOWESS-smoothed curves but rather the simple binned averages. We created 16 bins of hues and calculated the average spike rate for all stimulus presentations of those hues, then correlated the 16-dimensional tuning curve vector with the natural image tuning curves.

Natural scene models

Model scoring and cross validation:

We quantified how well the regression methods described neural responses by calculating the pseudo-R^2 score. This scoring function is applicable to Poisson processes, unlike a standard R^2 score (74). The pseudo-R^2 was calculated in terms of the log likelihood of the true neural activity $L(y)$, the log likelihood of the predicted output $L(\hat{y})$, and the log likelihood of the data under the mean firing rate $L(\bar{y})$.

$$R^2 = 1 - \frac{\log L(y) - \log L(\hat{y})}{\log L(y) - \log L(\bar{y})} = \frac{\log L(\hat{y}) - \log L(\bar{y})}{\log L(y) - \log L(\bar{y})}$$

The pseudo-R^2 is, at left, one minus the ratio of the deviance of the tested model to the deviance of the null model. It can be also be seen, at right, as the fraction of the maximum potential log-likelihood. It takes a value of 0 when the data is as likely under the tested model as the mean rate, and a value of 1 when the tested model perfectly describes the data.

We used 8-fold cross-validation (CV) when assigning a final score to the models. The input and spike data were segmented randomly by fixation into eight equal partitions. The methods were trained on seven partitions and tested on the eighth, and this was repeated until all segments served as the test partition once. We report the mean of the eight scores. If the monkey fixated on a single image more than once, all fixations were placed into the same partition. This ensures that the test set contains only images that were not used to train the model.

Hue models

The uniform field linear model, the generalized linear hue model, and the nonlinear hue model all describe neural activity as a function of the hues present in the receptive field on each fixation. To build the histograms, we calculated the hue angle of each pixel in CIELUV space, and then calculated the number of pixels in each of 16 bins of hues. Note that a hue is defined for a pixel even if it is quite desaturated. To ensure near-gray pixels would not affect the results, we weighted the contribution of each pixel to the histogram by its saturation (defined as the distance of the color from the L axis). Since the hue histograms have 16 bins, the base regression problem to describe neural activity from hue is 16-dimensional.

The uniform field model, presented in Figure 1F, is a linear model whose coefficients are set from the uniform field tuning curve. Inference is performed via a dot product of the coefficients with the hue histogram. This is, we multiplied the mean firing rate observed for a bin of hues by how much that hue bin is present in the receptive field, and then summed across hue bin. We then added a constant term to account for the difference in mean firing rate across contexts.

The generalized linear model (GLM) was a linear-nonlinear model with an exponential link function and a Poisson loss. We included elastic net regularization, and selected the regularization coefficient for each neuron using cross-validation in an inner loop. We implemented this with the R package r-glmnet (75). For our nonlinear model, we selected the machine learning method of gradient boosted decision trees as implemented by XGBoost, an open-source Python package (76). This method allows a Poisson loss function and has previously been shown to be effective in describing neural responses (62). Briefly, XGBoost trains multiple decision trees in sequence, with each trained on the errors of the previous trees. We chose several regularization parameters using Bayesian optimization for a single neuron. These parameters included the number of trees to train (200), the maximum depth of each decision tree (3), the data subsampling ratio (0.5), the minimum gain (0.3), and the learning rate (0.08).

To build tuning curves from the fit GLM and XGBoost models, we predicted the response to a vector indicating which color was present (that is, a "one-hot" vector with one entry per hue that is all zeros except for the hue that is present). Then, to estimate the measurement error of the tuning curves, we refit the models to the original neural responses resampled with replacement. This resulted in tuning curves from hundreds of bootstrapped model fits. In figures in which we display the tuning curves, the lower and upper error bounds represent the 5th and 95th percentiles of the tuning curves observed when refitting the models to the resampled data.

CNN model

Our convolutional neural network (CNN) encoding model was based on previously published studies in which it was shown that the intermediate layers of pretrained networks are highly predictive of V4 responses (5). Ours was built from the VGG16 network, which is a large convolutional network trained to classify the images from the ImageNet dataset (77). It contains 13 convolutional layers and 3 fully connected layers. We built an encoding model for each neuron from the activations of layer 14 (the first fully-connected layer). Layer 15 but not the output layer yielded similar predictive power. We did not modify or refit this CNN to predict neural responses. Instead, we ran nonlinear Poisson regression (XGBoost) to predict each neuron's response to an image from the values of layer 14 when the VGG network was given the same image. We found XGBoost to offer better predictions than other Poisson regression models. The final model thus takes a fixation image as input, runs the image through 14 layers of the VGG16 CNN, and then through a trained instance of XGBoost to predict the spike rate of a neuron. We call the combination of the CNN model and the trained XGBoost for each neuron the "CNN model".

The CNN model could then be used to build tuning curves. We conceptualized this as extracting the average first-order effect of hue upon the responses of this model to natural images. We perform the following cross-validated procedure for each of 8 bins of hues. First, we train the CNN model (i.e. train the XGBoost regressor) on the training set of the natural image dataset. We then modify the test set images by slightly desaturating all pixels whose hue lies within the current hue bin. The bins were chosen to be large (8 in instead of 16) to so as to be less affected by pixel noise and to speed computation. We desaturated by moving along the L axis of the LUV color space, the same color space in which we define hue. For robustness, we modified images at each of many desaturation levels, ranging from 5% to 100% desaturation. We then obtained the predictions of the CNN model to the original test set and also for each modified, desaturated test set, and take the average difference of these two predictions across all images. This process is repeated in an 8-fold cross-validation procedure, so that each image serves as the test set once. The resulting series of average differences can be plotted against the desaturation. The slope of this line represents the average first-order contribution of that bin of hues to the images in the dataset. Note that the value of slope reflects the scale the x-axis, which represents the parameterization of the desaturation percentage. It is best to think of the units of slope as arbitrary; the important result is the relative value of the slope between hues. Finally, the process was repeated for each bin of hues, resulting in the tuning curve to hue.

We sought to validate this procedure on simulated data. One important aspect is that predictions are made on images that are as close to the distribution of images in the training set as possible. Since images in which a single bin of hues are desaturated by 5% are visually indistinguishable from the originals, this is not likely to be a concern. Nevertheless, we observed whether this method would be able to reconstruct the hue tuning of simulated neurons. We constructed 20 simulated neurons that responded linearly to the hues present in a receptive field. Each neuron was cosine tuned with a randomly selected hue angle. Linear regression could perfectly reconstruct the hue tuning of these simulated neurons, as expected. The CNN method could also reconstruct the tuning curves, though less well than linear regression (as indicated by the spread of cross-validated pseudo-R^2 values, Supp. Fig. 3). If linear tuning curves do exist, then, the CNN method would be able to reconstruct them.

Calculation of error bounds

Each estimate of a tuning curve represents, in essence, a summary statistic of noisy data. To estimate error bounds on tuning curves, we relied on the nonparametric method of bootstrapping across trials, or for summary statistics of the entire neural population, additionally bootstrapping across neurons. Since the uniform field hue tuning curves used for correlations were simple averages of spike rates, binned over hue, we bootstrapped across trials to compute the confidence intervals. The natural scene tuning curves for the GLM and nonlinear methods represented the predicted response to single hues. For these methods, we computed uncertainty bounds on their predictions to single hues by retraining the methods on resampled datasets (with replacement) and selecting the 5^{th} and 95^{th} percentiles of the predicted output for each bin. For the CNN method, the tuning curves were calculated from linear fits of the difference in test set predictions as a function of hue bin desaturation. The difference in predictions was noisy across images, with large changes predicted for some images but small changes predicted for other images. This noise presented as uncertainty in the linear fit to the data. The error on the CNN tuning curve, then, represented the uncertainty in the linear fit to the test set predictions.

The uncertainty on each of the tuning curves was then propagated into the correlation between the natural scene and uniform field tuning curves. This was again done through bootstrapping. For a given natural scene/uniform field correlation, we correlated the natural scene and uniform field tuning curves from hundreds of model fits upon resampled data, yielding a large distribution of correlations. We then reported the mean, 5^{th}, and 95^{th} percentiles of

this distribution. The uncertainty of the mean across neurons included a bootstrap across the trials used to build the tuning curves for each neuron, followed by a bootstrap across neurons.

References

1. Carandini M, Demb JB, Mante V, Tolhurst DJ, Dan Y, Olshausen BA, et al. Do we know what the early visual system does? Journal of Neuroscience. 2005;25(46):10577-97.
2. Hegdé J, Van Essen DC. Strategies of shape representation in macaque visual area V2. Visual neuroscience. 2003;20(3):313-28.
3. Pasupathy A, Connor CE. Shape representation in area V4: position-specific tuning for boundary conformation. Journal of neurophysiology. 2001;86(5):2505-19.
4. Hung CP, Kreiman G, Poggio T, DiCarlo JJ. Fast readout of object identity from macaque inferior temporal cortex. Science. 2005;310(5749):863-6.
5. Yamins DL, Hong H, Cadieu CF, Solomon EA, Seibert D, DiCarlo JJ. Performance-optimized hierarchical models predict neural responses in higher visual cortex. Proceedings of the National Academy of Sciences. 2014;111(23):8619-24.
6. Connor CE, Brincat SL, Pasupathy A. Transformation of shape information in the ventral pathway. Current opinion in neurobiology. 2007;17(2):140-7.
7. Logothetis NK, Sheinberg DL. Visual object recognition. Annual review of neuroscience. 1996;19(1):577-621.
8. Simoncelli EP, Olshausen BA. Natural image statistics and neural representation. Annual review of neuroscience. 2001;24(1):1193-216.
9. Vinje WE, Gallant JL. Sparse coding and decorrelation in primary visual cortex during natural vision. Science. 2000;287(5456):1273-6.
10. David SV, Vinje WE, Gallant JL. Natural stimulus statistics alter the receptive field structure of v1 neurons. Journal of Neuroscience. 2004;24(31):6991-7006.
11. Touryan J, Felsen G, Dan Y. Spatial structure of complex cell receptive fields measured with natural images. Neuron. 2005;45(5):781-91.
12. David SV, Gallant JL. Predicting neuronal responses during natural vision. Network: Computation in Neural Systems. 2005;16(2-3):239-60.
13. Felsen G, Dan Y. A natural approach to studying vision. Nature neuroscience. 2005;8(12):1643.
14. Olshausen BA, Field DJ. What is the other 85 percent of V1 doing. L van Hemmen, & T Sejnowski (Eds). 2006;23:182-211.
15. Bashivan P, Kar K, DiCarlo JJ. Neural population control via deep image synthesis. Science. 2019;364(6439):eaav9436.
16. Cowley B, Williamson R, Clemens K, Smith M, Byron MY, editors. Adaptive stimulus selection for optimizing neural population responses. Advances in neural information processing systems; 2017.
17. David SV, Hayden BY, Gallant JL. Spectral receptive field properties explain shape selectivity in area V4. Journal of neurophysiology. 2006;96(6):3492-505.
18. Oleskiw TD, Pasupathy A, Bair W. Spectral receptive fields do not explain tuning for boundary curvature in V4. Journal of neurophysiology. 2014;112(9):2114-22.
19. Touryan J, Mazer JA. Linear and non-linear properties of feature selectivity in V4 neurons. Frontiers in systems neuroscience. 2015;9:82.
20. Zeki SM. Colour coding in rhesus monkey prestriate cortex. Brain research. 1973;53(2):422-7.
21. Desimone R, Schein SJ. Visual properties of neurons in area V4 of the macaque: sensitivity to stimulus form. Journal of neurophysiology. 1987;57(3):835-68.
22. Carlson ET, Rasquinha RJ, Zhang K, Connor CE. A sparse object coding scheme in area V4. Current Biology. 2011;21(4):288-93.
23. Popovkina DV, Bair W, Pasupathy A. Modeling diverse responses to filled and outline shapes in macaque V4. Journal of neurophysiology. 2019;121(3):1059-77.
24. Watanabe M, Tanaka H, Uka T, Fujita I. Disparity-selective neurons in area V4 of macaque monkeys. Journal of Neurophysiology. 2002;87(4):1960-73.
25. Hinkle DA, Connor CE. Disparity tuning in macaque area V4. Neuroreport. 2001;12(2):365-9.
26. Hinkle DA, Connor CE. Three-dimensional orientation tuning in macaque area V4. Nature neuroscience. 2002;5(7):665.
27. Mountcastle VB, Motter B, Steinmetz M, Sestokas A. Common and differential effects of attentive fixation on the excitability of parietal and prestriate (V4) cortical visual neurons in the macaque monkey. Journal of Neuroscience. 1987;7(7):2239-55.
28. Roe AW, Chelazzi L, Connor CE, Conway BR, Fujita I, Gallant JL, et al. Toward a unified theory of visual area V4. Neuron. 2012;74(1):12-29.
29. Conway BR, Moeller S, Tsao DY. Specialized color modules in macaque extrastriate cortex. Neuron. 2007;56(3):560-73.

30. Tanigawa H, Lu HD, Roe AW. Functional organization for color and orientation in macaque V4. Nature neuroscience. 2010;13(12):1542-8.
31. Conway BR, Tsao DY. Color-tuned neurons are spatially clustered according to color preference within alert macaque posterior inferior temporal cortex. Proceedings of the National Academy of Sciences. 2009;106(42):18034-9.
32. Li M, Liu F, Juusola M, Tang S. Perceptual color map in macaque visual area V4. Journal of Neuroscience. 2014;34(1):202-17.
33. Bohon KS, Hermann KL, Hansen T, Conway BR. Representation of perceptual color space in macaque posterior inferior temporal cortex (the V4 Complex). Eneuro. 2016;3(4):ENEURO. 0039-16.2016.
34. Kusunoki M, Moutoussis K, Zeki S. Effect of background colors on the tuning of color-selective cells in monkey area V4. Journal of Neurophysiology. 2006;95(5):3047-59.
35. Portilla J, Simoncelli EP. A parametric texture model based on joint statistics of complex wavelet coefficients. International journal of computer vision. 2000;40(1):49-70.
36. Okazawa G, Tajima S, Komatsu H. Image statistics underlying natural texture selectivity of neurons in macaque V4. Proceedings of the National Academy of Sciences. 2015;112(4):E351-E60.
37. Osorio D, Vorobyev M. A review of the evolution of animal colour vision and visual communication signals. Vision research. 2008;48(20):2042-51.
38. Seung HS, Sompolinsky H. Simple models for reading neuronal population codes. Proceedings of the National Academy of Sciences. 1993;90(22):10749-53.
39. Wang Z, Stocker AA, Lee DD, editors. Optimal neural population codes for high-dimensional stimulus variables. Advances in neural information processing systems; 2013.
40. Brunel N, Nadal J-P. Mutual information, Fisher information, and population coding. Neural computation. 1998;10(7):1731-57.
41. Finkelstein A, Ulanovsky N, Tsodyks M, Aljadeff J. Optimal dynamic coding by mixed-dimensionality neurons in the head-direction system of bats. Nature communications. 2018;9(1):3590.
42. Bushnell BN, Pasupathy A. Shape encoding consistency across colors in primate V4. Journal of neurophysiology. 2012;108(5):1299-308.
43. Chelazzi L, Della Libera C, Sani I, Santandrea E. Neural basis of visual selective attention. Wiley Interdisciplinary Reviews: Cognitive Science. 2011;2(4):392-407.
44. Motter BC. Neural correlates of attentive selection for color or luminance in extrastriate area V4. Journal of Neuroscience. 1994;14(4):2178-89.
45. Mirabella G, Bertini G, Samengo I, Kilavik BE, Frilli D, Della Libera C, et al. Neurons in area V4 of the macaque translate attended visual features into behaviorally relevant categories. Neuron. 2007;54(2):303-18.
46. Kastner S, Pinsk MA, De Weerd P, Desimone R, Ungerleider LG. Increased activity in human visual cortex during directed attention in the absence of visual stimulation. Neuron. 1999;22(4):751-61.
47. Connor CE, Preddie DC, Gallant JL, Van Essen DC. Spatial attention effects in macaque area V4. Journal of Neuroscience. 1997;17(9):3201-14.
48. Connor CE, Gallant JL, Preddie DC, Van Essen DC. Responses in area V4 depend on the spatial relationship between stimulus and attention. Journal of neurophysiology. 1996;75(3):1306-8.
49. Gallant JL, Connor CE, Rakshit S, Lewis JW, Van Essen DC. Neural responses to polar, hyperbolic, and Cartesian gratings in area V4 of the macaque monkey. Journal of neurophysiology. 1996;76(4):2718-39.
50. Bushnell BN, Harding PJ, Kosai Y, Bair W, Pasupathy A. Equiluminance cells in visual cortical area V4. Journal of Neuroscience. 2011;31(35):12398-412.
51. Zeki S. The representation of colours in the cerebral cortex. Nature. 1980;284(5755):412-8.
52. DiCarlo JJ, Cox DD. Untangling invariant object recognition. Trends in cognitive sciences. 2007;11(8):333-41.
53. Grill-Spector K, Weiner KS. The functional architecture of the ventral temporal cortex and its role in categorization. Nature Reviews Neuroscience. 2014;15(8):536.
54. Heeger DJ. Normalization of cell responses in cat striate cortex. Visual neuroscience. 1992;9(2):181-97.
55. Knierim JJ, Van Essen DC. Neuronal responses to static texture patterns in area V1 of the alert macaque monkey. Journal of Neurophysiology. 1992;67(4):961-80.
56. Sillito A, Jones H. Context-dependent interactions and visual processing in V1. Journal of Physiology-Paris. 1996;90(3-4):205-9.
57. Fitzpatrick D. Seeing beyond the receptive field in primary visual cortex. Current opinion in neurobiology. 2000;10(4):438-43.
58. McClure Jr JP, Polack P-O. Pure tones modulate the representation of orientation and direction in the primary visual cortex. Journal of neurophysiology. 2019;121(6):2202-14.
59. Yeh C-I, Xing D, Williams PE, Shapley RM. Stimulus ensemble and cortical layer determine V1 spatial receptive fields. Proceedings of the National Academy of Sciences. 2009;106(34):14652-7.
60. Heitman A, Brackbill N, Greschner M, Sher A, Litke AM, Chichilnisky E. Testing pseudo-linear models of responses to natural scenes in primate retina. bioRxiv. 2016:045336.
61. McIntosh L, Maheswaranathan N, Nayebi A, Ganguli S, Baccus S, editors. Deep learning models of the retinal response to natural scenes. Advances in neural information processing systems; 2016.

62. Benjamin AS, Fernandes HL, Tomlinson T, Ramkumar P, VerSteeg C, Chowdhury RH, et al. Modern machine learning as a benchmark for fitting neural responses. Frontiers in computational neuroscience. 2018;12.
63. Ponce CR, Xiao W, Schade P, Hartmann TS, Kreiman G, Livingstone MS. Evolving super stimuli for real neurons using deep generative networks. bioRxiv. 2019:516484.
64. Felsen G, Touryan J, Dan Y. Contextual modulation of orientation tuning contributes to efficient processing of natural stimuli. Network: Computation in Neural Systems. 2005;16(2-3):139-49.
65. Pospisil DA, Pasupathy A, Bair W. 'Artiphysiology'reveals V4-like shape tuning in a deep network trained for image classification. Elife. 2018;7:e38242.
66. Morcos AS, Barrett DG, Rabinowitz NC, Botvinick M. On the importance of single directions for generalization. arXiv preprint arXiv:180306959. 2018.
67. Smith MA, Sommer MA. Spatial and temporal scales of neuronal correlation in visual area V4. Journal of Neuroscience. 2013;33(12):5422-32.
68. Snyder AC, Morais MJ, Smith MA. Dynamics of excitatory and inhibitory networks are differentially altered by selective attention. Journal of neurophysiology. 2016;116(4):1807-20.
69. Shoham S, Fellows MR, Normann RA. Robust, automatic spike sorting using mixtures of multivariate t-distributions. Journal of neuroscience methods. 2003;127(2):111-22.
70. Kelly RC, Smith MA, Samonds JM, Kohn A, Bonds A, Movshon JA, et al. Comparison of recordings from microelectrode arrays and single electrodes in the visual cortex. Journal of Neuroscience. 2007;27(2):261-4.
71. Brainard DH, Vision S. The psychophysics toolbox. Spatial vision. 1997;10:433-6.
72. Bondar IV, Leopold DA, Richmond BJ, Victor JD, Logothetis NK. Long-term stability of visual pattern selective responses of monkey temporal lobe neurons. PloS one. 2009;4(12):e8222.
73. McMahon DB, Jones AP, Bondar IV, Leopold DA. Face-selective neurons maintain consistent visual responses across months. Proceedings of the National Academy of Sciences. 2014;111(22):8251-6.
74. Cameron AC, Windmeijer FA. An R-squared measure of goodness of fit for some common nonlinear regression models. Journal of Econometrics. 1997;77(2):329-42.
75. Friedman J, Hastie T, Tibshirani R. Regularization paths for generalized linear models via coordinate descent. Journal of statistical software. 2010;33(1):1.
76. Chen T, Guestrin C, editors. Xgboost: A scalable tree boosting system. Proceedings of the 22nd acm sigkdd international conference on knowledge discovery and data mining; 2016: ACM.
77. Simonyan K, Zisserman A. Very deep convolutional networks for large-scale image recognition. arXiv preprint arXiv:14091556. 2014.
78. Sánchez-Montañés MA, Pearce TC. Why do olfactory neurons have unspecific receptive fields? Biosystems. 2002;67(1-3):229-38.
79. Rigotti M, Barak O, Warden MR, Wang X-J, Daw ND, Miller EK, et al. The importance of mixed selectivity in complex cognitive tasks. Nature. 2013;497(7451):585.

Supplementary information

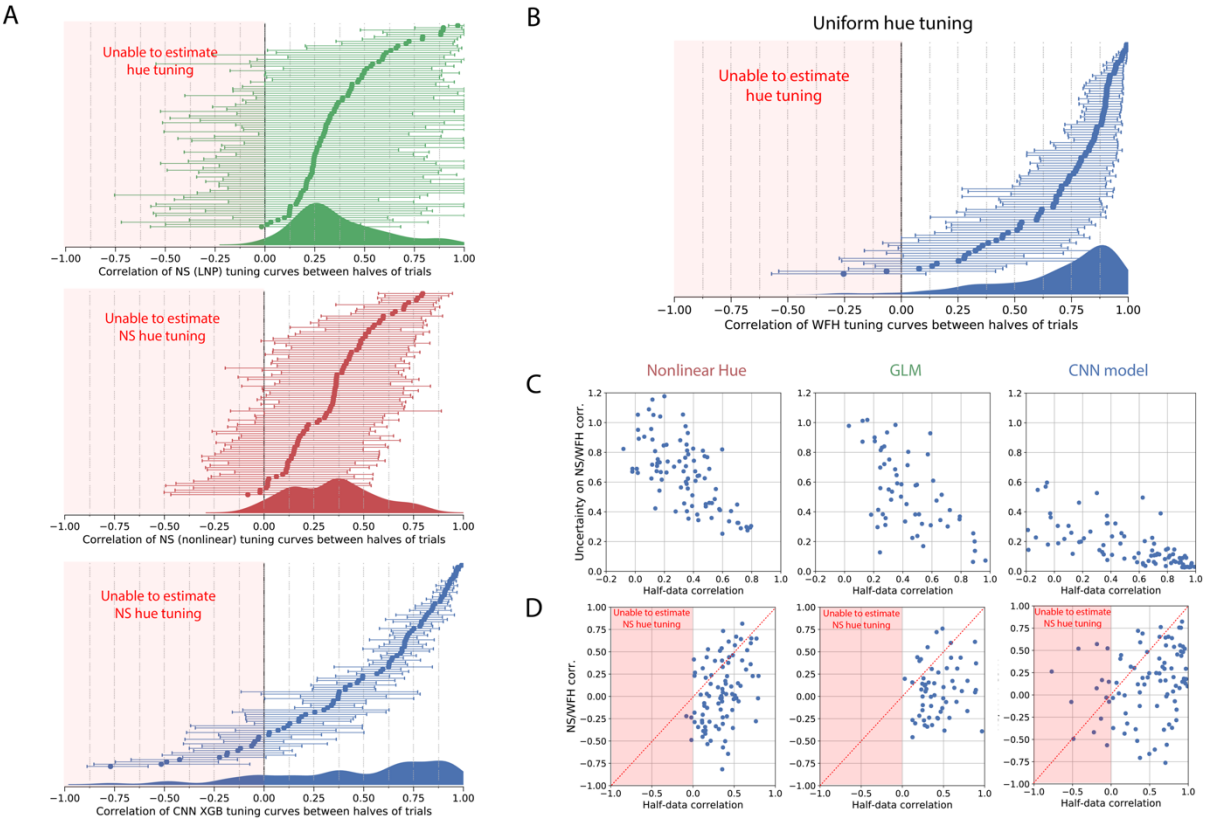

Figure S1. Our ability to estimate hue tuning can be captured by the correlation of the tuning estimated on two non-overlapping halves of the trials. This correlation would be 1 in the no-noise or infinite-data condition. For a single neuron, the half-trial correlation represents an estimate of what natural scene/uniform hue tuning curve correlations we would observe if hue tuning did not change between conditions. (Note that by fitting models on only half of the data, the estimate of hue tuning is noisier than in the full-data tuning estimation. Our actual ability to measure hue tuning is thus better than communicated by this control. For this reason these plots show a *lower bound* of the correlation we would expect if hue tuning were the same across conditions.) **A**) For the GLM hue model (green), the nonlinear hue model (red) and the CNN model (blue), these plots display the correlation of the tuning estimated on two non-overlapping halves of the trials. One can also consider this test as running 2-fold cross-validation and comparing the tuning curves estimated on both splits of data. Like in the main analysis, we split the data such that all trials (fixations) on the same image were placed in the same fold of data. In this plot the neurons are again ordered by their correlation to produce a cumulative distribution (the order of neurons is not the same as in Figures 2C and 4A). Errors show 5th and 95th percentiles of this procedure repeated on the original data resampled with replacement. The smoothed distributions projected below are reproduced in Figures 2C and 4A. **B)** The half-trial control for the uniform hue condition. This communicates how precisely we can estimate uniform hue tuning. The errors again derive from repeating the cross-half correlation when resampling the trials and re-splitting the data in half. **C)** The estimation error as communicated by these half-data control captures the same sources of variability that were incorporated into the principle uncertainty measure of the correlation between tuning curves (e.g. Figure 2Bii). That uncertainty was measured by resampling the trials, then re-calculating and re-correlating the tuning curves. To demonstrate this, here we show the relation between the half-data correlation and the size of the uncertainty bars from the main figures (Figures 2C and 4A). As expected, there is a strong negative correlation. Higher half-data correlations for a neuron correspond to smaller bounds of the natural scene/uniform hue correlation. **D)** Here we compare, neuron-by-neuron, the relationship between the half-data correlation and the natural scene/uniform hue correlation. (Panel A only communicates the difference in overall distributions.) Importantly, there is little relation

between the half-data correlation (i.e. our ability to estimate natural scene hue tuning) and the natural scene/uniform hue correlation (i.e. whether we observed that neuron to shift tuning). This shows when we observe a shift in hue tuning, it is not simply because for that neuron we poorly estimated the natural scene hue tuning. Another key takeaway is the number of neurons that lie in the region below the dotted red line, where the split-trial correlation is higher than the natural scene/uniform hue correlation. For all three estimation methods (nonlinear hue, GLM hue, and CNN model), significantly more neurons lie below this line than above it.

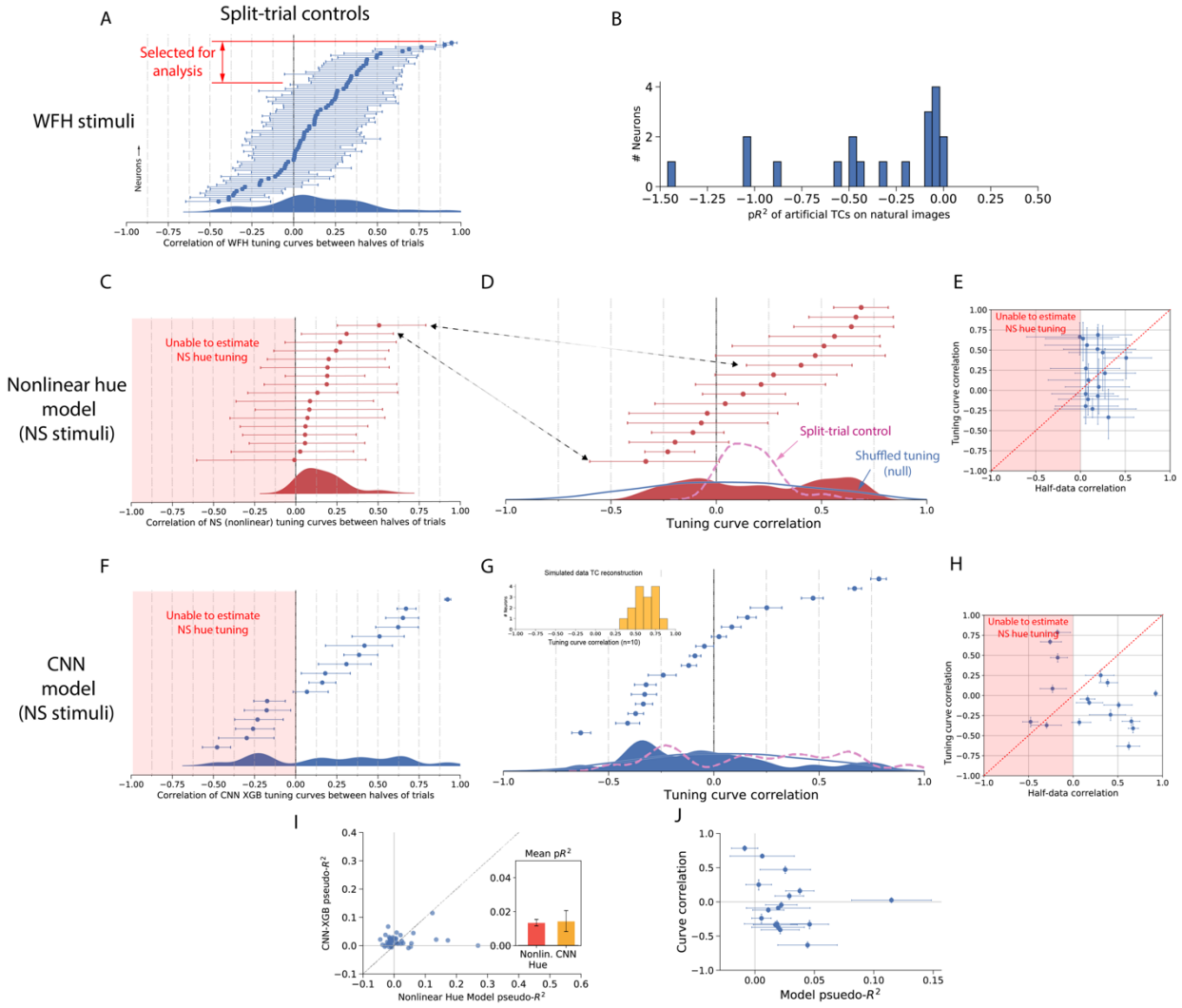

Figure S2: Collected data for Monkey 2. M2 differed from M1 in that its gaze was fixed at image center, rather than free viewing. The data for M2 was recorded in a single session and included significantly fewer trials than M1. **A)** Most neurons in M2 showed poor hue tuning, and we were not able to consistently estimate uniform hue hue tuning nearly as well as for M1. Displayed here is the split-trial control, in which for each of 80 neurons we correlate the uniform hue tuning curves estimated on non-overlapping halves of trials (compare to Fig. S1b for M1). For later analysis, we only selected neurons for which we could consistently estimate hue tuning, i.e. the tuning curves built from non-overlapping halves of trials significantly correlated (95% CI non-inclusive of 0). **B**) Like for M1, the uniform hue tuning curves were worse at predicting natural scene responses than the mean firing rate on natural scenes.

C-E) *Analysis of the natural scene tuning curves estimated by the nonlinear hue model was inconclusive*. Note that we did not analyze the GLM hue model for M2 because it could poorly explain responses on held-out trials (Supp. Fig. S3c). **C**) The split-trial control for tuning curves estimated from the nonlinear hue model (i.e. the correlations of natural scene tuning curves estimated on non-overlapping halves of trials). The natural scene tuning curves could not

be estimated as consistently as for M1 (in Fig. S1a). **D**) The natural scene/uniform hue tuning curve correlations as estimated by the nonlinear hue model. Like for M1 (Fig. 2c) we overlay the split-trial distribution and the null distribution expected with random reshuffling of hue tuning. The arrows indicate the two neurons for which the split-trial control was significantly above 0. **E)** Neuron-by-neuron comparisons for the hue model of the natural scene/uniform hue correlations and the split-trial correlations. A neuron has a lower natural scene/uniform hue correlation than the split-trial correlation (which is a lower bound of what the natural scene/uniform hue correlation would be if hue tuning did not change) when it lies below the dotted red y=x line. While some neurons lie below, nearly an equal number lie above. By a Wilcoxon signed rank test, we were unable to reject the null hypothesis that natural scene/uniform hue correlations are lower than the split-trial correlations (p=0.65). Overall, it was not clear from the hue model on M2 neurons whether hue tuning does or does not change.

F-J) *Parallel analysis of the natural scene tuning curves estimated with the CNN method*. **F)** Like for the hue model, our estimation ability was much poorer than for M1, but the distribution of correlations of hue tuning estimated of non-overlapping halves of trials was skewed towards positive correlations. **G)** Natural scene/uniform hue correlations. Like for M1 (Fig. 4a) we overlay the split-trial distribution. Inserted is the distribution of natural scene/uniform hue correlations of simulated neurons with cosine hue tuning. (Since M2 saw 10x fewer trials than M1, we re-calculated our estimation ability on this smaller dataset. For 10 simulated neurons, the method could indeed reconstruct tuning curves, though less well than with the trials for M1 (Fig. S5).) **H)** Neuron-by-neuron comparisons for the CNN model of the natural scene/uniform hue correlations and the split-trial correlations. This time, among the neurons for which we could consistently estimate hue tuning (i.e. with a positive correlation of tuning curves estimated on split data), all neurons had a higher split-trial natural scene curve correlation than a natural scene/uniform hue correlation. This was significant under a Wilcoxon signed rank test at p=0.003. Note additionally that there was little relation between the half-data correlation (i.e. our ability to estimate natural scene hue tuning) and the natural scene/uniform hue correlation (i.e. whether we observed that neuron to shift tuning). Thus, among neurons for which we could consistently estimate both uniform hue tuning and natural scene tuning (i.e. both split-trial correlations significantly above 0), hue tuning changed across conditions. **I)** The cross-validated pseudo-R^2 scores captured how well the natural scene models can explained data on held-out trials. In general the scores were much lower than for M1 (Fig. 3b). There were some neurons the hue model explained better (lying below the y=x line), and many neurons quite poorly predictable from hue were better predicted by the CNN model (those near the origin, which lie above the y=x line). **J)** As for M1 (Fig. 3e), the pseudo-R^2 score of the CNN model on a given neuron was not predictive of the natural scene/uniform hue correlation.

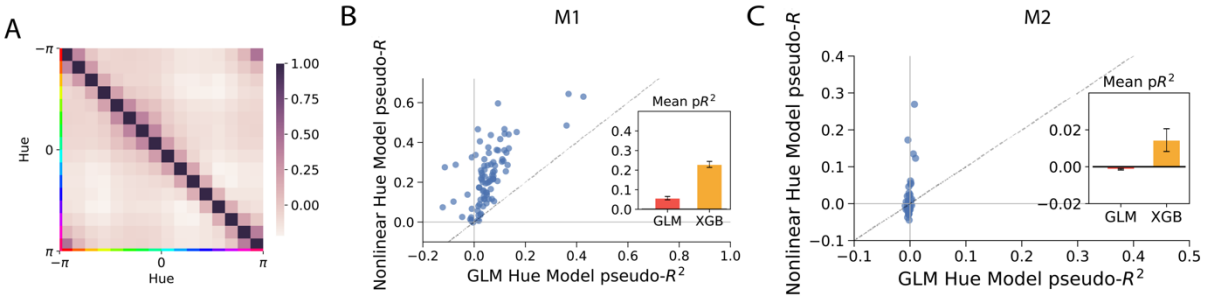

Figure S3. The response of V4 neurons to hue is nonlinear and contains interactions between bins of hues. A) The correlation matrix of hues on the natural image dataset observed by M1. Since the off-diagonal terms are not zero, there are correlation between hues (especially of similar colors). These correlations could bias the tuning curve of a linear fit if nonlinear hue interactions exist in the neural response. As shown in (B) and in (C), these interactions do indeed exist. This can be seen by the fact that the nonlinear model (gradient boosted trees, XGB) predicts neural activity better than the generalized linear model (GLM) when both are fed the (saturation-weighted) histograms of hues present within the receptive field during each fixation.

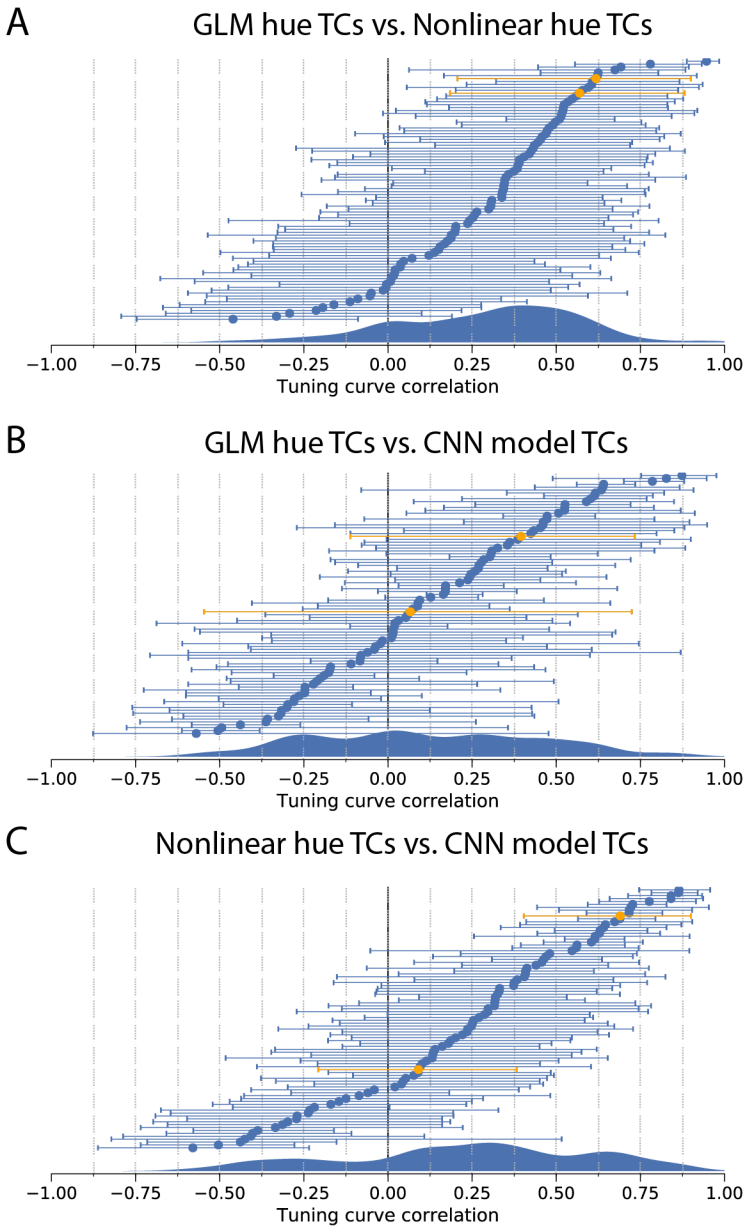

Figure S4. Correlation of the tuning curves (TCs) constructed from natural stimuli across methods. A) Correlations between the TCs found via the linear and nonlinear hue models. B) Correlations between the TCs found via the linear hue model and the VGG CNN curve construction method. C) Correlations between the TCs found via the nonlinear hue model and the VGG CNN curve construction method.

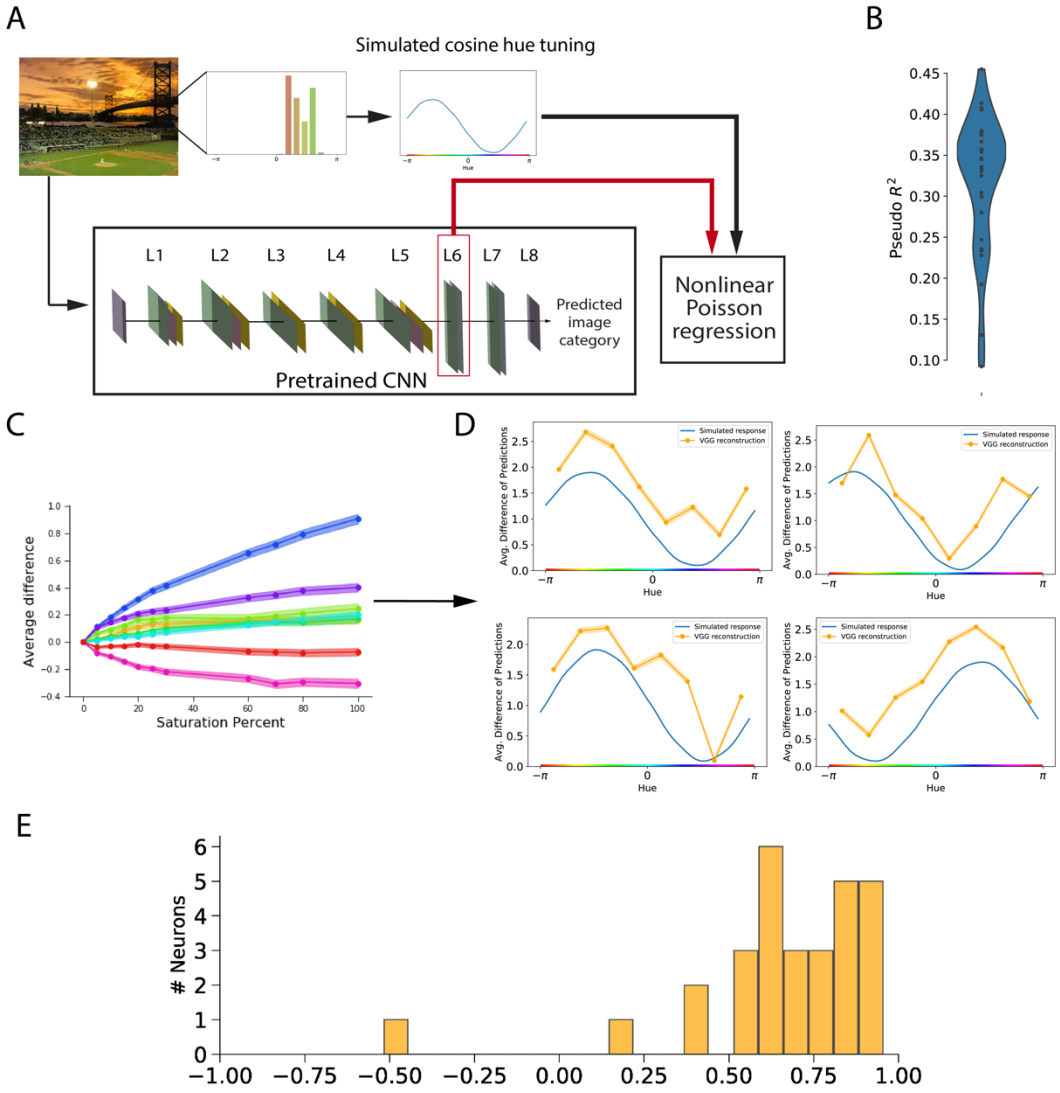

Figure S5. Reconstructing simulated neural responses shows that the CNN method can in principle observe hue tuning. A) As for the main model, we fit a nonlinear Poisson regression model to predict 'neural' responses from the intermediate activations of the VGG16 model when given image segments. Instead of the actual neural response, here we fit to a simulated neural response, which comprised of a random (fixed) cosine filter applied to the distribution of hues in each fixation. B) The model could predict these simple responses well, but not perfectly, with typical pseudo-R^2 scores less than 0.4. C) Once again we calculated the average difference in predictions between held-out images and those same images but with each of 8 bins of hues desaturated by some percentage. We plot the difference in response as a function of desaturation. It can be seen that the line is somewhat sub-linear, like for actual neural responses. This plot proves that some of this sub-linearity is not neural in origin, but rather a function of both our choice of color space (CIELUV) and the way that the VGG model incorporates color into the response. D) Tuning curves constructed in this way (from the slopes of the saturation dependencies) closely resemble the original filters, with some noise. E) The typical noise of this method's reconstruction of tuning curves can be summarized as a distribution of tuning curve correlations. This distribution is the point of comparison, representing what distribution we would expect if hue tuning were unchanged between categories of stimuli.

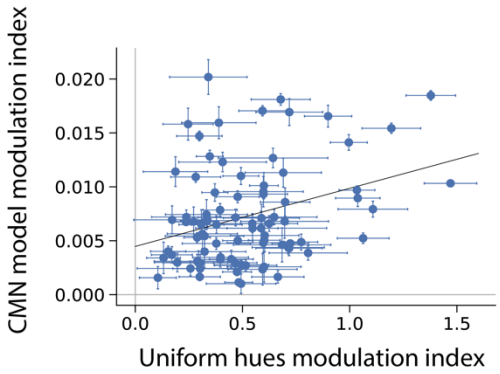

841

842 **Figure S6:** We calculated a modulation index measuring how drastically hue affected the V4 response on either
843 uniform hues or natural images. In uniform hues, the modulation index was defined as the maximum of the uniform
844 hue tuning curve, minus the minimum, and divided by the mean spike rate. In natural scenes, we examined how
845 strongly various hues affected the CNN model response. This was measured by the difference between the maximum
846 and the minimum of the CNN model tuning curve, which, measuring a difference in the predictions rather than the
847 absolute value, is already mean-normalized. There was a weak correlation (p=0.003) between these two indices.

848

Appendix: why mixed selectivity?

The visual cortex is faced with the task of representing aspects of the visual world in the activity of its neurons. Visual information can be broken down into separate features, with potentially overlapping information content. These features might be hue, shape, or other visual aspects. What is the optimal way of representing M features in a single population of N neurons? Here we argue that, under certain reasonable assumptions, each neuron within a population should respond to multiple features.

Denote the features describing behaviorally-relevant aspects of the world as $\boldsymbol{\theta} = \{\theta_1, \theta_2, \ldots, \theta_M\}$. We are interested in how well $\boldsymbol{\theta}$ can be decoded from the population activity of N neurons $\boldsymbol{x} = \{x_1, x_2, \ldots, x_N\}$, given the quality of the neural representation. To this end, we seek to bound the error of the best possible decoder. We will quantify the error as the mean-squared error over all features θ_i:

$$\sigma^2 = \left\langle \left(\boldsymbol{\theta} - \widehat{\boldsymbol{\theta}}\right)^2 \right\rangle = \sum_i^M \left\langle \left(\theta_i - \hat{\theta}_i\right)^2 \right\rangle$$

where $\langle \cdot \rangle$ denotes the expectation over the stimulus distribution, and $\widehat{\boldsymbol{\theta}}$ are the decoded features.

A common way to bound this error is to invoke the Cramer-Rao inequality (38):

$$\left\langle \left(\boldsymbol{\theta} - \widehat{\boldsymbol{\theta}}\right)^2 \right\rangle \geq tr(\boldsymbol{F}(\boldsymbol{\theta})^{-1}).$$

This states that the reconstruction error is lower-bounded by the inverse of the Fisher information of the neural population with respect to $\boldsymbol{\theta}$. The Fisher information at a given value of $\boldsymbol{\theta}$ is defined as $\boldsymbol{F}(\boldsymbol{\theta}) = \langle \boldsymbol{\nabla_\theta}(\boldsymbol{x}) \boldsymbol{\nabla_\theta}(\boldsymbol{x})^T \rangle$, or element-wise for each pair of features i, j as:

$$F(\theta)_{i,j} = \left\langle \left(\frac{\partial}{\partial \theta_i} \ln p(\boldsymbol{x}|\theta_i)\right) \cdot \left(\frac{\partial}{\partial \theta_j} \ln p(\boldsymbol{x}|\theta_j)\right) \right\rangle_{\boldsymbol{x}}.$$

Thus, maximizing the Fisher information minimizes the mean error of a good decoder (i.e. one that saturates the Cramer-Rao bound). The Fisher information also serves as a bound upon the mutual information between θ and $\boldsymbol{x}$ (39).

When the noise on neurons is Gaussian with equal variance, the Fisher information simplifies and can be written in terms of the variance σ of the noise and the individual activation functions f:

$$F(\boldsymbol{\theta}) = \sum_i^N \sigma^{-1} \nabla_\theta f_i(\boldsymbol{\theta}) \, \nabla_\theta f_i(\boldsymbol{\theta})^T.$$

If the neural response is Poisson, with mean rate given by the activation, the Fisher is the related quantity

$$\nabla F(\boldsymbol{\theta}) = \sum_i^N f_i(\boldsymbol{\theta})^{-1} \nabla_\theta f_i(\boldsymbol{\theta}) \, \nabla_\theta f_i(\boldsymbol{\theta})^T.$$

Now, given this Fisher, what distribution of response selectivity minimizes the Cramer-Rao bound? For any one parameter θ_k, the kth diagonal element of the Fisher (which limits the variance of the error on θ_k) is proportional to $\sum_i^N \left(\frac{\partial f_i(\boldsymbol{\theta})}{\partial \theta_k}\right)^2$ in the case of Gaussian noise and $\sum_i^N \frac{1}{f_i(\boldsymbol{\theta})} \left(\frac{\partial f_i(\boldsymbol{\theta})}{\partial \theta_k}\right)^2$ in the case of Poisson neurons. To say precisely what $f_i(\boldsymbol{\theta})$ maximizes this term requires making some assumptions about both allowable f_i and the distribution of $\boldsymbol{\theta}$. We will review a handful of settings below. However, it is clear that this sum will be larger if many neurons are sensitive to θ_k. This is, intuitively, why mixed selectivity helps.

Depending on the form of the tuning curves f_i, however, a neuron may face a tradeoff between having high $\frac{\partial f_i(\boldsymbol{\theta})}{\partial \theta_k}$ for different θ_k. This is plausible, especially if we consider that the total magnitude of the gradient is bounded to some finite value. Thus, it is theoretically possible that coding for other variables decreases one's sensitivity to a first variable to a prohibitive degree. We are interested here in determining which distributions over $\boldsymbol{\theta}$ have this property, given some assumptions about the form of $f_i(\boldsymbol{\theta})$. In general, if the f_i are neural tuning functions parameterized by $\boldsymbol{\lambda}$, a neural population will not have mixed selectivity when, even at the point when all neurons only tune for one variable, the gradient (with respect to the tuning parameters) of the kth diagonal element of the inverse Fisher (corresponding to a single variable) is larger than the magnitude of the gradient of all other elements corresponding to the other variables:

$$|\nabla_\lambda [F(\boldsymbol{\theta})^{-1}]_{kk}| > \left|\nabla_\lambda \sum_{m \neq k}^{M} [F(\boldsymbol{\theta})^{-1}]_{mm}\right|$$

When this condition is met, one can increase decoding accuracy by making neurons more tuned to single features. If this condition is met even when neurons already tune to just one feature each, then no neuron will have mixed selectivity. We posit that this is extremely unlikely; a great number of neurons coding with small sensitivity to a feature is generally going to have higher Fisher information than just one neuron coding strongly for that feature, if the number of neurons is large.

The exact conditions will depend on the form of $\boldsymbol{\theta}$ and $f_i(\boldsymbol{\theta})$. Other papers have taken a similar approach in various circumstances. (78) demonstrated that if neurons are linear, then mixed selectivity is empirically optimal, but the assumptions about the data distribution are not clearly stated. (41) show that for uniform distributed circular variables and von Mises tuning curves, mixed selectivity yields higher Fisher information. (39) investigated the situation in which M neurons encode M variables, and furthermore each neuron is a linear-nonlinear map with non-decreasing scalar link h and linear weight matrix W: $f_i(\boldsymbol{\theta}) = h(\boldsymbol{W^T\theta})$. In this circumstance, the authors found that in the optimal mapping of Gaussian $\boldsymbol{\theta}$ the weight vectors are projections in the distribution of $\boldsymbol{\theta}$ with small variance, with some repulsion between weight vectors. Thus, in order for mixed selectivity to not be optimal in this circumstance, the variables should entirely decorrelated and mutually orthogonal. This is not the case for typical visual descriptors; color and hue correlate with objects and scenes in many ways.

It is interesting to contrast this approach to a different approach justifying nonlinear mixed selectivity. One line of reasoning from the behavior literature is that nonlinear mixed selectivity allows a greater diversity of linear readouts, and thus behaviors (79). Thus, while here we maximize the *potential quality* of the readout, one also finds a benefit for nonlinear mixed selectivity when considering only the *overall number* of potential readouts.

References

Finkelstein A, Ulanovsky N, Tsodyks M, Aljadeff J. 2018. Optimal dynamic coding by mixed-dimensionality neurons in the head-direction system of bats. *Nature communications* 9: 3590

Rigotti M, Barak O, Warden MR, Wang X-J, Daw ND, et al. 2013. The importance of mixed selectivity in complex cognitive tasks. *Nature* 497: 585

Sánchez-Montañés MA, Pearce TC. 2002. Why do olfactory neurons have unspecific receptive fields? *Biosystems* 67: 229-38

Seung HS, Sompolinsky H. 1993. Simple models for reading neuronal population codes. *Proceedings of the National Academy of Sciences* 90: 10749-53

Wang Z, Stocker AA, Lee DD. *Advances in neural information processing systems2013*: 297-305.